Overview of Midfrequency Reverberation Data Acquired During the Target and Reverberation Experiment 2013

Jie Yang, Dajun Tang, Brian T. Hefner, Kevin L. Williams, and John R. Preston, *Member, IEEE*

***Abstract*—The Target and Reverberation EXperiment 2013 (TREX13) included a comprehensive reverberation field project in the frequency band of 2–10 kHz, and was carried out off the coast of Panama City, FL, USA, from April 21 to May 17, 2013. A spatially fixed transmit and receive acoustic system was used to measure reverberation over time under diverse environmental conditions, allowing study of reverberation level (RL) dependence on bottom composition, sea surface conditions, and water column properties. Extensive in situ measurements, including a multibeam bathymetric survey, chirp sonar subbottom profiling, gravity/diver cores, sediment sound speed and attenuation, interface roughness, wind-generated sea surface waves, and water column properties, were made to support studies of environmental effects on RL. Beamformed RL data are categorized to facilitate studies emphasizing physical mechanisms of 1) bottom reverberation; 2) sea surface impact; and 3) biological impact. This paper is an overview of RL over the entire sea trial, intending to summarize major observations and provide both a road map and suitable data sets for follow-up efforts on model/data comparisons. Emphasis is placed on the dependence of RL on local geoacoustic properties and sea surface conditions.**

***Index Terms*—Biologics, bottom-dominated reverberation, midfrequency reverberation, rough sea surface, Target and Reverberation EXperiment 2013 (TREX13), target echo.**

I. Introduction

UNDERWATER reverberation measurements date back to the 1940s [1]–[3] when the study of reverberation was still in its infancy with little environmental characterization. From the early 1990s, there have been a series of well-organized multi-institutional and multinational reverberation experiments. The first one was the Acoustic Reverberation Special Research Program (ARSRP) sponsored by the Office of Naval Research (ONR), in 1991 and 1993, respectively, on the west flank of the Mid-Atlantic Ridge [4]–[7]. The next two major experiments in this series were called Rapid Response (RR, 1996–1998), which was related to the NATO Rapid Environmental Assessment (REA) effort [8]–[12], and the Boundary Characterization Experiment (BCE, 2000–2004, [12]–[15]). In addition, another reverberation experiment, the Acoustic Clutter Reconnaissance Experiment (ACRE), was carried out in the STRATA FORmation on Margins (STRATAFORM) area in 2001 [16].

ARSRP was designed to study long-range bottom dominated reverberation at low frequencies (<1 kHz), with a focus on reverberation amplitude, range dependence, and correlation to bottom topography. The experiment was carried out in an area called the Atlantic Natural Laboratory with nominal water depth of 3300–5200 m and an area of 270 km × 470 km. It was found from multiple studies [5]–[7] that reverberation correlates with bottom topography in a positive way, i.e., protrusions in bathymetry cause high backscatter/reverberation. This correlation was confirmed through modeling as well. By using the supporting fine-scale bottom bathymetric data and removing the effects of propagation, reverberation data were also used to estimate scattering strength (SS) as a function of grazing angle [17].

The main goal of the RR/REA field experiments was to validate the practicality of using directional reverberation data as an operational remote sensing tool. The series of experiments in 1996–1998 were carried out in the Mediterranean and west Atlantic continental shelves [10], [12] covering the frequency band of 160–4000 Hz and water depths of 1320–3200 m. A network for reverberation data transfer was set up with Supreme Allied Commander Atlantic acting as the data fusion center. Manual inversion was employed to provide a map of bottom loss and SS.

The ACRE focused on naturally occurring heterogeneities, i.e., geologic clutter, which includes both surficial and buried features. These features contribute significantly to backscatter and therefore can result in false target detections. The goal was to measure and understand high returns in reverberation from geologic clutter to mitigate/distinguish them from man-made objects. The experiment was carried out in the STRATAFORM area on the New Jersey shelf with varying water depths of 50–250 m in the low-to-midfrequency band (100–3500 Hz).

Among these reverberation experiments, the one most relevant to this work is the BCE carried out in 2000–2002. The main goal of the experiment was to identify and measure key factors of ocean boundaries, with an emphasis on the bottom in the frequency band of 500–5000 Hz. A series of experiments were conducted at three sites: the Malta Plateau, New Jersey Shelf, and Scotian Shelf with supporting environmental data including multibeam bathymetry, chirp subbottom profiling, localized bottom reflection and scattering measurements, coring, and grab

Manuscript received January 31, 2017; revised June 29, 2017 and November 3, 2017; accepted February 1, 2018. Date of publication March 16, 2018; date of current version July 12, 2018. *(Corresponding author: Jie Yang.)*

Associate Editor: P. Theobald.

J. Yang, D. Tang, B. T. Hefner, and K. L. Williams are with the Applied Physics Laboratory, University of Washington, Seattle, WA 98105 USA (e-mail: jieyang@apl.washington.edu; djtang@apl.washington.edu; hefner@apl.washington.edu; williams@apl.washington.edu).

J. R. Preston is with the Applied Research Laboratory, Pennsylvania State University, State College, PA USA (e-mail: jrp7@arl.psu.edu)

Digital Object Identifier 10.1109/JOE.2018.2802578

samples. To explore bottom properties and their acoustic effects, areas with sand (with and without ripple fields), thick mud deposits, rock outcrops, and fine layering, were sampled. Using new boundary measurement techniques, it was found that the subbottom structure dominated the interaction between acoustics and the seabed over a large part of Malta Plateau, while bubble clouds dominated at low-to-moderate grazing angles when the sound interacts with the sea surface [13].

From these previous reverberation experiments, substantial knowledge was gained in terms of the spatial, temporal, and frequency dependence of long-range reverberation at low-to-mid frequencies. Spatial and temporal variations of the environment were demonstrated to be critical in understanding reverberation and improving prediction capabilities. However, there lacked a midfrequency (2–10 kHz) shallow-water reverberation experiment, where the acoustic system was fixed in space with companion high-resolution environmental measurements, from the sea surface down to subbottom heterogeneities, sampled at the appropriate scales to allow constrained model/data comparison. A fixed acoustic measuring system allows signal variation due to true environmental variation to be definitely separated from the effect of moving sensors. The fixed system and adequate environmental data provide a means to improve quantitative understanding of the various physical mechanisms relevant to reverberation and thus improve model prediction capabilities.

ONR Ocean Acoustic Program sponsored a major field experiment called the Target and Reverberation EXperiment in 2013 (TREX13). The main goal of TREX13 was to contemporaneously measure acoustic and environmental data at midfrequencies (2–10 kHz) in shallow water so that detailed model/data comparison could be achieved and important environmental parameters could be identified.

The design philosophy of TREX13 centered around the sonar equation expressed in decibels: $\mathrm{RL} = \mathrm{SL} - 2\mathrm{TL} + \mathrm{ISS}$, where RL is the reverberation level, SL the source level, TL the transmission loss, and ISS the integrated SS (the SS properly integrated over incident and scattered angles over the active area of the transmitted signal). To achieve a full understanding of RL, all components in the sonar equation were measured. Specifically, RL was measured using a spatially fixed-fixed source/receive array system producing beamformed RL along different bearings. TL was measured in two ways: one used moored vertical line arrays and a towed source, and the other used a receiving system on a moving vessel. The latter, the so-called "ping-pong run," consists of measurements of two-way TL and concurrent reverberation: one-way TL from a fixed-source to receiver on a moving vessel, one-way TL back to a fixed-array near the source (ship-received signal transmitted back to a fixed-array), and concurrent reverberation received on the fixed-array [18]. With additional inputs of SS, this type of data completes the sonar equation. The SS was independently measured after the experiment using a direct path backscattering measurement technique [19].

The TREX13 site had an approximate water depth of 19 m. The SLs allowed reverberation to be measured to a maximum range of 7 km, with the first 5 km being the focus of environmental measurements. This depth allowed diver support for both array deployment and environmental measurements. The main transmission path of the TREX13 site was about 2 km from shore, and the water column during the experiment was typically well mixed with a mild thin bottom layer.

Extensive environmental information supporting each component in the sonar equation was measured. Measurements included the directional surface wave spectrum [20], fine-scale bathymetry and backscatter intensity at 400 kHz [21], bottom roughness spectra [22], direct path bottom backscatter intensity [19], subbottom chirp survey [23], sediment sound speed and attenuation [24], ambient noise [25], water column properties, and sediment transport [26]. In addition, array beamforming allowed the associated environmental measurements to be limited to particular tracks (azimuthal angles), thus greatly reducing the environmental measurement effort. For TREX13, most environmental characterization focused on two tracks of interest: the "main reverberation" and "clutter" tracks. Details are given in Section II.

This paper provides an overview of TREX13 reverberation data acquired over the entire experiment and a road map for follow-on efforts on data/model comparison. In particular, to achieve quantitative understanding of different physical mechanisms, data are categorized into reverberation that I) is bottom-dominated; II) includes significant sea surface impacts; and III) includes significant biological impacts. Major observations of each category are presented, and data sets suitable for modeling purposes in categories I and II are identified. Supporting environmental data useful for subsequent modeling efforts are presented in conjunction with major observations. There was also a stationary, passive acoustic target (PAT) deployed along the main reverberation track. Preliminary target echo analysis from the PAT is presented, emphasizing its sensitivity to environmental changes such as rough sea surface conditions and warming/cooling of the water column.

This paper is organized as follows. A summary of TREX13 is given in Section II. Section III provides an overview of TREX13 reverberation data as functions of time, space, and environmental conditions. The categorization of reverberation data is presented in Section IV as are the major conclusions for each category. Section V investigates one prominent feature of RL, i.e., its fluctuations, and its correlation to bathymetry. Preliminary analysis of target echo from the PAT is presented in Section VI. The echo signal-to-noise ratio (SNR) and arrival time are shown to closely correlate to environmental changes. To provide background for future understanding/modeling efforts, a discussion is given in Section VII on the link between major observations and resulting research questions generated by TREX13 reverberation data and supporting environmental measurements. A summary is given in Section VIII. Finally, the Appendix presents details of acoustic systems including sources, receiving arrays, their geometries, transmitted waveforms with SLs, and an array beam pattern discussion.

II. TREX13 Reverberation Experiment

The main part of TREX13 was carried out off the coast of Panama City, FL, USA, from April 21 to May 17, 2013. The

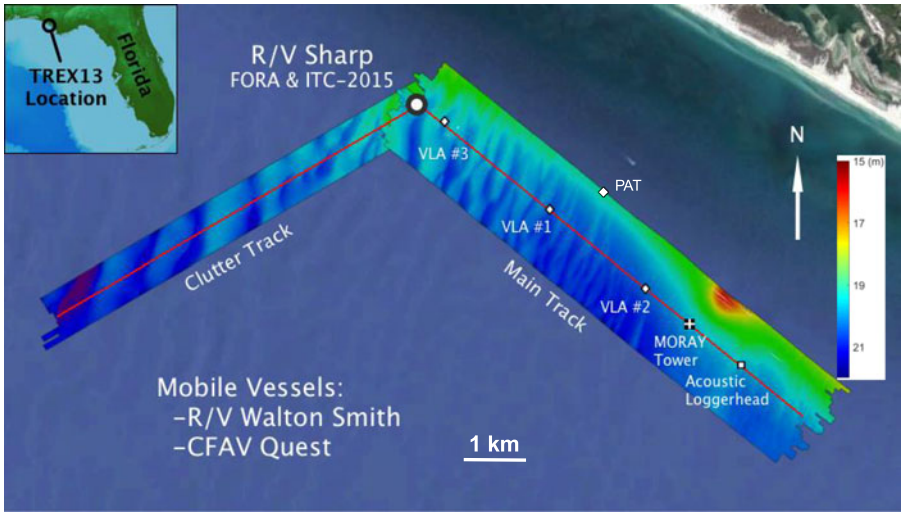

Fig. 1. TREX13 experimental site with fine scale bathymetric data collected from a multibeam sonar survey (see [21]) along both the main and clutter tracks with the colorbar representing water depth. Assets were deployed along the main reverberation track, including three vertical line arrays (VLA #1–#3), MORAY tower, and an acoustic loggerhead. The MORAY tower has a vector sensor and horizontal and vertical hydrophone arrays, with the lowest sensors mounted 3 m above the bottom. The acoustic loggerhead is a self-recording hydrophone mounted 1 m above the bottom on a simple frame. The Passive Acoustic Target (PAT) was deployed about 2.8 km from the *R/V Sharp*.

experimental site, shown in Fig. 1, was located approximately 2-km offshore from Shell Island near Panama City Beach, FL, USA. The *R/V Sharp*, location shown in Fig. 1, was placed in a four-point moor when on site and the bottom-mounted sources and receive arrays were deployed from this platform. Extending out from the location of the *R/V Sharp* were the main reverberation and the clutter tracks. The main reverberation track was oriented roughly along shore at a bearing of 129°, with water depth of about 19 m, while the clutter track was approximately perpendicular to shore and the water depth varied from 19 to 23 m. The main reverberation track was 7 km long and 1.4 km wide, with extensive environmental measurements covering the first 5 km. The background color along the two tracks shows the fine-scale bathymetric data from a multibeam survey with the colorbar representing water depth [21]. The bathymetric data show corrugation of the seafloor near the main reverberation track, especially within 3 km of the *R/V Sharp* location. This corrugation has a peak-to-trough bathymetric variation of roughly 1 m over a spatial scale of 200–300 m. These features are less pronounced further along the track and eventually disappear 5 km from the *R/V Sharp*. The clutter track shows similar features but the bathymetric change is over a larger spatial scale.

The two tracks were chosen to study different aspects of reverberation. The main reverberation track was chosen for its roughly range-independent environment with water depth of 19 ± 1 m. Data collected along this track, with the support of extensive environmental measurements, are especially suitable for understanding and quantitatively modeling reverberation under known environmental conditions. The clutter track has several known clutter objects including bridge sections and ship wrecks that are of interest for target detection modeling. Many assets were deployed along the main reverberation track to measure TL and bistatic reverberation (see Fig. 1). These assets included three moored vertical line arrays, a bottom-mounted vector sensor (MORAY tower), and an autonomous acoustic recorder (acoustic loggerhead). An air-filled target PAT, which served as a known reference target, was also deployed along this track.

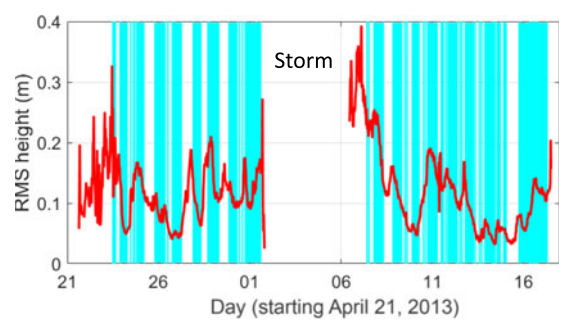

Fig. 2. RAS active transmission periods (cyan) throughout TREX13 with sea surface RMS height superimposed (red).

Two acoustic systems were used to measure reverberation and details of both systems are given in the Appendix. All data presented in this paper came from one of the two systems, the so-called Reverberation Acoustic System (RAS). RAS refers to the combination of an ITC2015 source and a triplet receive array ([15]; see parts A and B in the Appendix for details). The source and the receive array were connected to the *R/V Sharp* and mounted at fixed positions above the seafloor. The array was deployed horizontally 2.1 m above the seafloor, clipped on a line which was supported by two poles. The source was mounted on a pedestal 1.2 m above the seafloor near the array. In contrast to a towed scenario, the unique fixed-fixed setup reduced any uncertainties due to source and receiver motion.

Acoustic signals were transmitted from RAS both day and night from April 21 to May 17, 2013 with a gap occurring May 1–6, due to a storm event, during which the *R/V Sharp* left the experimental site. Total data coverage spanned 250 h. Fig. 2

summarizes the acoustic measurements over time and accompanying sea surface conditions. The transmission schedule of reverberation signals is overlaid with the sea surface root-mean-square (RMS) height [27] measured by a directional surface wave buoy over the course of the experiment [20]. As can be seen in the figure, reverberation data were recorded under calm (close to zero RMS height) to modestly rough (RMS height of 0.25 m) sea surface conditions. Unfortunately, no data under significant wind conditions were recorded because the *R/V Sharp* could not be kept in the moored configuration during the high wind period. A complete list of transmitted waveforms and their SLs are given in the Appendix.

III. Overview of TREX13 Reverberation Data

During TREX13, acoustic data were recorded day and night to measure reverberation over time under diverse environmental conditions, allowing the study of RL dependence on bottom composition, sea surface conditions, and water column properties. An overview of the reverberation data is given in this section. Measured on the triplet array, acoustic data were first matched filtered and beamformed to give absolute RL over 360° of look angles.

In this section, the analysis focuses on the 2.7–3.6-kHz linear-frequency-modulated (LFM) signal to present the main characteristics of the reverberation since it was transmitted consistently throughout the experiment and its bandwidth is such that it provides good resolution of features in the reverberation. The overall RL characteristics are presented as functions of time, space (range and bearing), and environmental conditions. Dominant contributors, which impact reverberation, include scattering from the sea bottom, air/water surface, and biologics in the water column. An overall variation in mean RL, i.e., range-averaged RL trend, for TREX13 was found to be 17 dB at 3-km range due to all factors that contribute to alter reverberation. Persistent and pronounced RL fluctuations were observed throughout the experiment with fluctuation levels that varied over the course of the experiment. Note, RL variation in this paper refers to slow time changes while RL fluctuation corresponds to fast time or spatial changes.

A. Reverberation Data Processing

The triplet array data were matched filtered and beamformed to give absolute RL along any bearing within 360° [28]. A frequency-domain matched filter was used here and defined as

$$d(t) = F^{-1}\left\{G(f) \times S(f) \times A(f)^{*}\right\} \tag{1}$$

where $G(f)$ is a Gaussian shape filter with full 3-dB width defined as the bandwidth of the transmitted waveform; $S(f)$ is the spectrum of the received signal; $A(f)^{*}$ is the conjugate of the spectrum of the drive voltage with its peak value normalized to unity; and $d(t)$ is the output time series after matched filtering. Note, the matched filter processing here uses the drive voltage as the replica, and therefore assumes negligible effects from the source TVR. The source TVR is presented in part A of the Appendix and a discussion on this assumption is given as well.

As an example, Fig. 3(a) shows the drive voltage before and after applying the matched filter using the 2.7–3.6-kHz, 1-s long LFM. Most in-band energy is preserved, and therefore, the pulse after matched filtering has a much higher peak. The advantage of this matched-filter is that it preserves the correct ambient noise level. The raw reverberation data (black) are compared in Fig. 3(b) to the same data that are filtered (blue) and matched filtered (red). During TREX13, data recording was set to start 1 s before acoustic transmission, and the first 1-s data were used to quantify ambient noise level for each ping. The raw data flatten out after 4 s due to out of band energy. The matched-filtered signal has been shifted to the center of the pulse for comparison and overlaps with the filtered signal. For this 2.7–3.6-kHz LFM signal, reverberation signal can be measured to about 8 s after filtering out the out-of-band noise.

A typical beamformed RL, a broadside beam in this case, is shown in Fig. 3(c). For this particular ping, the SL is 194.4 dB and the beamformed ambient noise level is about 55 dB re 1 μPa in the 2.7–3.6-kHz band. Note, this 55 dB represents the noise contribution along a particular beam, different from that measured by a single hydrophone, which records noise over the full 360°, as in Fig. 3(b). For example, at 3.5 kHz, the broadside beamwidth is about 2.2° and therefore, the beamformed ambient noise level is $10 \times \log_{10}(2.2/360) = -22.1$ dB relative to the ambient noise level seen in Fig. 3(b). The beamformed reverberation signal can be measured to about 8 s, equivalent to a one-way propagation distance of approximately 6 km, before falling below the ambient noise level.

In the beamforming process, the cardioid array beam pattern, discussed in detail in part E of the Appendix, can affect RL. As demonstrated by Haralabus *et al.*, [28], the beam at a particular look angle has the peak of its main lobe normalized to unity to ensure uniform target echo strength as the same target appears at different steering angles. As the main beam steers toward endfire, it widens and the widening results in higher RL if assuming a uniform distribution of scatterers causes reverberation. During TREX13, there were four source/receiver array geometries (see part C of the Appendix), with the main reverberation track appearing at different steering angles relative to endfire. The main reverberation track is rotated off endfire by 88°, 88°, 25°, and 47°, respectively. In this paper, the beam pattern widening effect is taken into account by referencing the integrated beam intensity to that at broadside. This is only done when comparing RL along the main reverberation track among different geometries.

In the following sections, all RL are referenced to an SL of 200 dB re 1 μPa at 1 m for all waveforms to facilitate comparison. The uniform SL compensates for small SL variation among waveforms and transmission at different times. SL for each waveform was calibrated during the experiment and details are given in part D of the Appendix. Specifically, RL is adjusted with a constant, which is the difference between the true SL of each signal and a reference SL of 200 dB re 1 μPa at 1 m. Note, the beamformed ambient noise level is altered in the same fashion due to SL compensation.

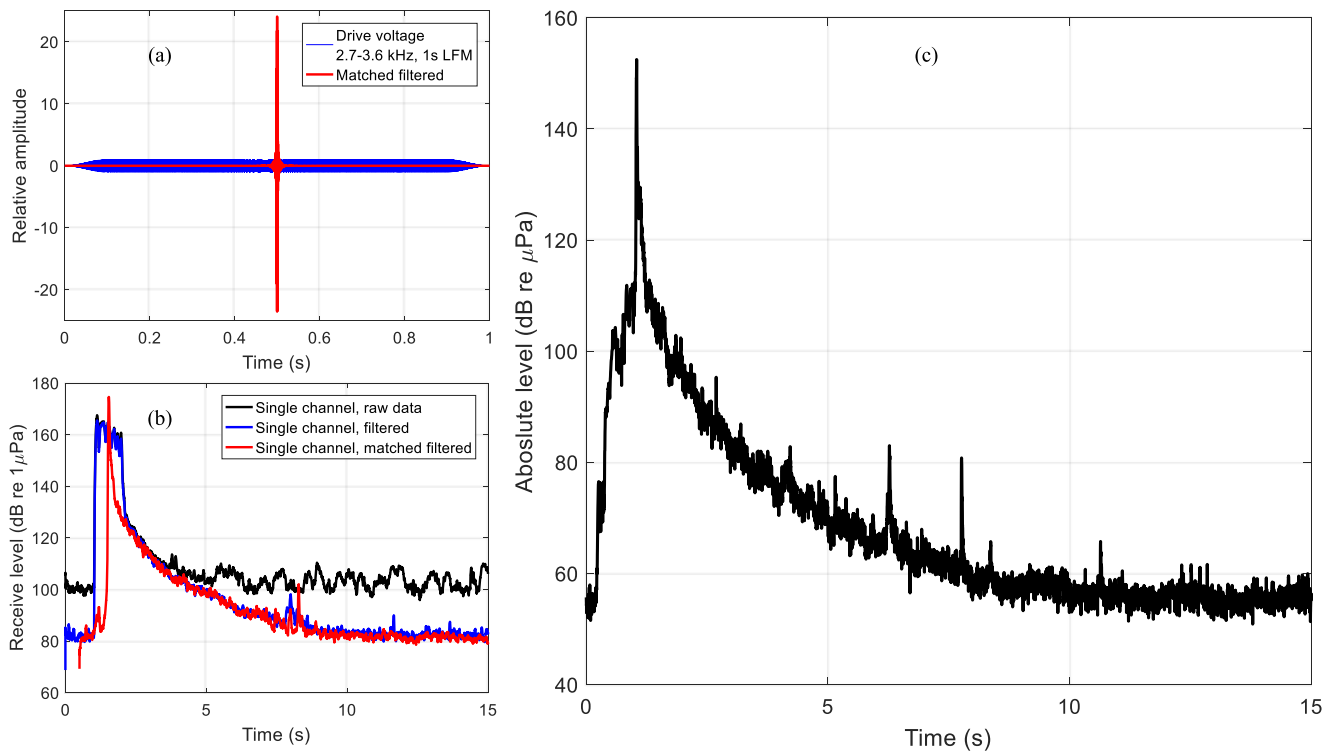

Fig. 3. (a) Normalized drive voltage (blue) and compressed pulse after matched filter (red). (b) Comparison of single channel reverberation data in raw (black), Gaussian filtered only (blue), and matched filtered (red) forms with 1 s of ambient noise at the beginning. (c) Beamformed RL for the beam looking along the 129° bearing. SL = 194.4 dB re 1 μPa at 1 m.

B. RL Dependence on Time, Range, and Bearing

To give a general picture of the characteristics of RL and its variation with time during TREX13, reverberation data from 12 overnight data sets are shown in Fig. 4. Each color panel represents one beamformed data set, which contains RL from a group of consecutive pings at the 129° bearing. The *x*- and *y*-axis correspond to slow and fast times respectively. The fast times are shown on a logarithmic scale to display the features more clearly at short ranges. The start time (local) and the number of hours each data set lasted are labeled at the top and bottom of each panel, respectively. The color bar is set to start from 50 dB re 1 μPa, the quietest beamformed ambient noise level observed during TREX13 for the 2.7–3.6-kHz signal.

In Fig. 4, stationary targets show up in the form of horizontal lines, i.e., they are fixed in space and therefore the echo returns have about the same arrival times. One example is the echo return from the vertical line array VLA#1 at around 3.15 s, corresponding to a one-way distance of 2.4 km. Occasional intensive biological activity can be observed, as in Panel 4, which will be discussed in more detail in Section IV. In this case, biological activity caused a 20-dB increase in RL and covered an area of approximately 3 km $\times$ 4 km. Shipping noise is observed in multiple data sets (panels 5–7, i.e., vertical stripes).

Spatial fluctuations in RL can be seen more clearly by removing the overall decay from the reverberation data. In Fig. 5, the general trend in the RL, i.e., $t^{-3.4}$, has been removed for all beams between the 109° and 149° bearings and the fluctuations are shown on a 10 dB scale. The features shown in Fig. 5 correspond to persistent fluctuation pattern in the RL that vary with both range and bearing and are observed throughout TREX13. This RL fluctuation pattern will be discussed in Sections III-B and V. The conversion from time to range is based on a constant in-water sound speed of 1525 m/s.

For RL that are recorded day and night under diverse environmental conditions, one important measure is the overall variation in mean RL due to all contributing factors including interactions with the sea surface, bottom, and biologics. To quantify the variation of the mean RL using the 2.7–3.6-kHz signal, the beamformed RL along the 129° bearing is first averaged over 300 m in range to smooth out the RL fluctuations. Then, data that showed 6 dB of beamformed RL above ambient noise were selected to exclude data that were ambient noise limited. The mean RL, as shown in Fig. 6, displays an overall 17-dB variation at 3 km throughout the experiment. In addition, within the 17-dB overall variation, the histogram of RL (shown in inset) demonstrates that most of the time, about 95%, RL falls in a 10-dB range of 76–86 dB re 1 μPa. The variation is due to a combination of mechanisms that affect the RL. To address different physical mechanisms, it thus becomes useful to delineate the data, isolating the mechanisms and environmental conditions that affect reverberation, to support modeling of each one individually. This naturally leads to a categorization of RL data, as discussed in Section IV.

C. Evolution of RL Fluctuation and Its Scattering Nature

The RL fluctuation pattern, as shown in Fig. 5, is consistently observed in almost all TREX13 data. While the locations of these fluctuations are persistent, their levels vary over the course

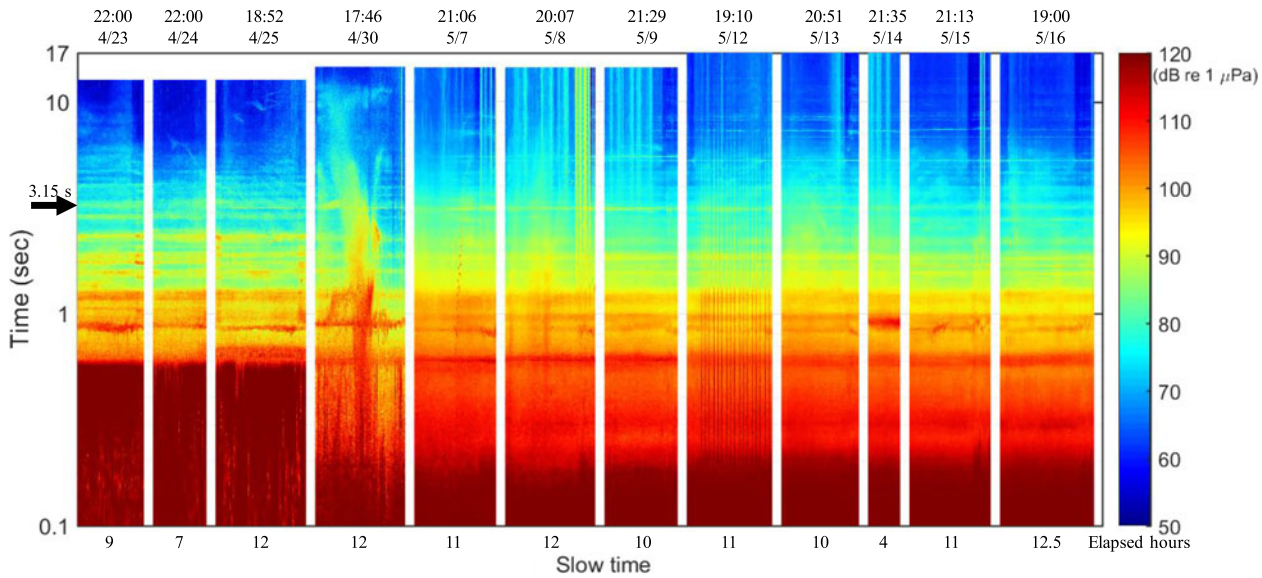

Fig. 4. Collection of RL from 12 overnight data sets, using 2.7–3.6-kHz LFM pulses, for the beam along the main reverberation track. Labeled above and below each panel are the local start time/date and the coverage in time of each dataset. The entire transmission time of the 12 overnight data sets is about 5.5 days. Fast time is plotted on the y-axis. SL = 200 dB re 1 μPa at 1 m. The white space in between data sets is for separation purpose only. The arrow at 3.15 s indicates scattered signal from the moored VLA#1 at 2.4-km. The storm occurred between the 4th and 5th panels.

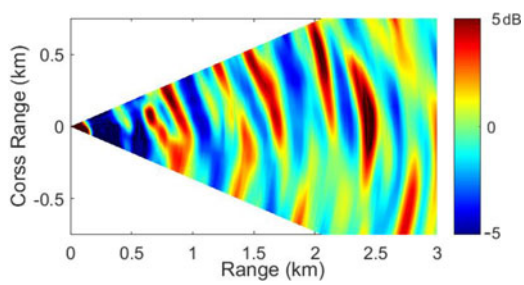

Fig. 5. RL fluctuation for beams in the bearing range 109°–149° re North collected on May 16. For clarity, the data have been rotated such that the beam along the main reverberation track is now parallel to the x-axis. This is an average of 10 pings using the 2.7–3.6-kHz LFM pulses.

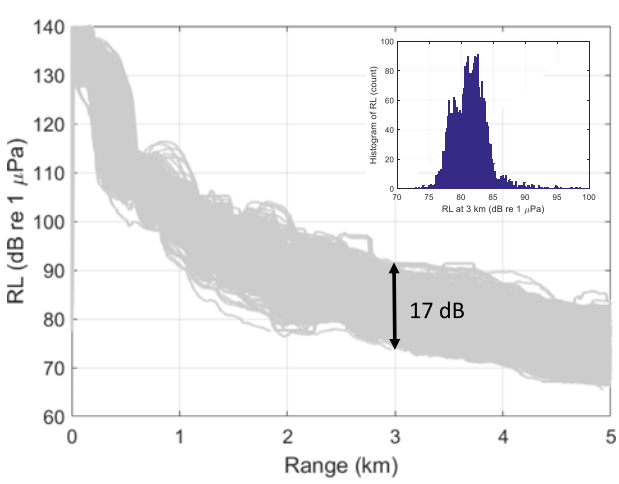

Fig. 6. All 2.7–3.6-kHz signals along 129° bearing with RL exceeding ambient noise level by 6 dB or more. At 3 km, RL displays a 17-dB variation throughout the experiment with 95% of RL in the range of 76–86 dB (histogram shown in insect). SL = 200 dB re 1 μPa at 1 m. The beam pattern widening effect has been accounted for, as detailed in part E of the Appendix, for the four geometries.

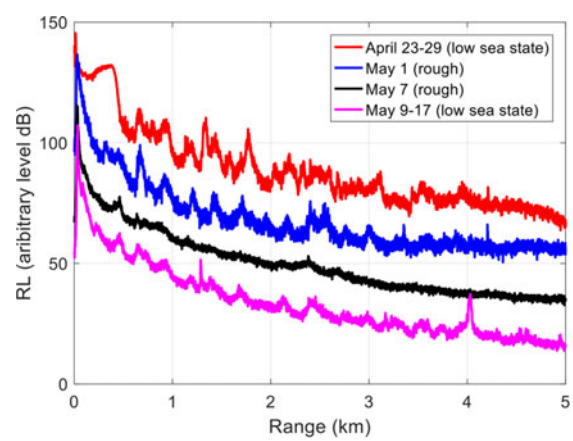

Fig. 7. Evolution of RL fluctuation during TREX13 for the 2.7–3.6-kHz waveform. The lower three curves have been shifted downward by 15, 35, and 50 dB for clarity. All curves are intensity averages of 10 pings beamformed along 129° bearing. The beam pattern widening effect has been accounted for, as detailed in part E of the Appendix, for the four geometries.

of the experiment. As will be shown in Section V, the fluctuation is deemed deterministic and correlates well with bathymetry. Four RL curves are shown in Fig. 7 in chronological order from top to bottom and are representative of data taken within the time periods of April 23–29, May 1, May 7, and May 9–17. All four curves are averages of 10 pings, beamformed along 129° bearing. The four representative curves display significant variation in RL fluctuation, i.e., peak-to-trough fluctuations for the first 3 km of the RL curves. Specifically, fluctuations started from a peak-to-trough level of 20 dB for the first week of the experiment, then reduced slightly on May 1, reached a minimum on May 7 after the six-day storm event, and then recovered and remained at a stable 10 dB for May 9–17. Note that data on May 1 and May 7 were both under rough sea surface conditions (see Fig. 2). The data on May 1 were ambient noise limited

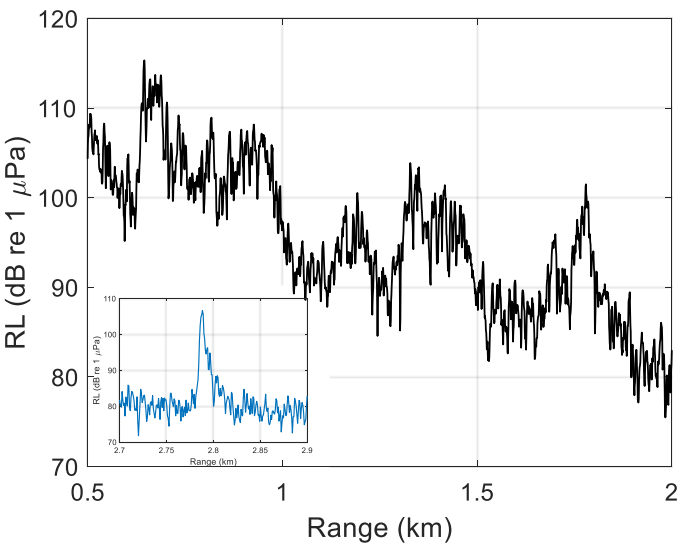

Fig. 8. Single ping beamformed RL showing fluctuations along the 129° bearing. The inset shows the echo from the PAT target, also a single ping, which has a much narrower width (20 m) than the fluctuations (200–300 m) along the main reverberation track. The 2.7–3.6-kHz LFM signal was used for both.

starting from about 3 km, mainly due to the rough sea surface (see Section IV-C).

One thing to clarify is that this variation is not due to RAS geometry changes (RAS geometries are given in the Appendix). The auxiliary system, presented in the Appendix as well, was never moved throughout the experiment and showed the same variation in fluctuation level. Fig. 8 compares the RL along the main reverberation track to the response of the air-filled PAT target. The RL slowly varies over the spatial scale of about 200–300 m. In contrast, the target echo from the PAT using the same waveform spans only 20 m. The hypothesis put forward based on this comparison is that RL comes from distributed instead of isolated target-like scatterers. Supporting environmental and acoustic data that help identify possible physical mechanisms responsible for the fluctuations are discussed in Section VII.

IV. RL Data Categorization

Because there are a number of mechanisms that cause RL variation, to achieve quantitative understanding of reverberation for each dominant mechanism, it is necessary to separate the TREX13 reverberation data into different categories. Three categories were chosen: I) bottom reverberation with a low sea state; II) bottom reverberation with a higher sea state; and III) reverberation that includes significant biological contributions. For each category, the categorization criteria and procedure are given, as well as observations and main conclusions. Most importantly, to support follow-on modeling efforts, the mean RL curves are given for categories I and II along the main reverberation track.

For category I and II data, the most challenging part is to identify RL data that satisfies the corresponding criteria but shows no observable biological activity. A procedure was developed to identify portions of RL data contaminated by biological scatterers, and then exclude the contaminated part from the data for categories I and II. Data presented here emphasize the frequency band of 2–4 kHz.

A. Criteria and Procedure

The criteria for the three categories are as follows. Category I is defined as bottom-dominated reverberation with low sea state (sea surface RMS height less than 0.1 m), low ambient noise, and no apparent biological activity. Category II has the same criteria as category I except for a rougher sea condition: The surface RMS height is greater than 0.1 m. Category III includes the data that have observable biological features that are transient in both time and space. The procedure used to categorize the RL data is to:

1) filter out the pronounced local biological features;
2) apply the surface RMS height condition using data from the directional wave buoys;
3) apply an ambient noise criterion, i.e., data are excluded when ambient noise level exceeds 60 dB re 1 μPa^2/Hz.

This level in general represents a relatively quiet coastal environment without apparent shipping noise.

For biological filtering, a procedure was developed to detect pronounced biological features by comparing data sets taken on different days and at different times of the day. The assumption is that biological activity is transient and while it may cause high reverberation, these levels will not persist over long periods of time (days). The comparison was carried out among all available data throughout TREX13 with surface RMS height less than 0.1 m, with the goal of finding the persistent background fluctuation pattern, as seen in Figs. 5 and 8. The data set that best represents the background fluctuation pattern was then selected. All other data sets were compared against the reference data set and a numerical threshold was imposed on the difference between the two. Transient features are identified if the difference exceeds the threshold and these features are removed from the data. This procedure detects and removes pronounced biological activity, which exceeds the threshold. No further adjustment is made for categories I and II data to account for the effects on propagation or longer range RL after going through biological congregate.

The biological filtering procedure was established using the waveform that has the most extensive temporal coverage: the 2.7–3.6-kHz LFM signal. The filtering results are extended to data of other waveforms, which either have a limited amount of data or lower resolution. This extension is applicable because of the structure of the transmission schedule. Since other waveforms are typically transmitted in an eight-waveform sequence, there is usually an accompanying, and therefore approximately concurrent, 2.7–3.6-kHz signal, and the filtering results of 2.7–3.6-kHz signal can be applied to other signals. Fig. 9 shows examples of RL before and after biological filtering using waveforms of 1.8–3.6-, 2.7–3.6-, and 3.4–3.5-kHz LFM, recorded during 05:30 – 06:30, April 24 (local time). It is found that about 19% of the data had noticeable biological impact and were filtered out by the procedure [see Fig. 9(b)]. A considerable portion that was filtered out comes from near range, where the wideband signals are saturated, not due to biologics.

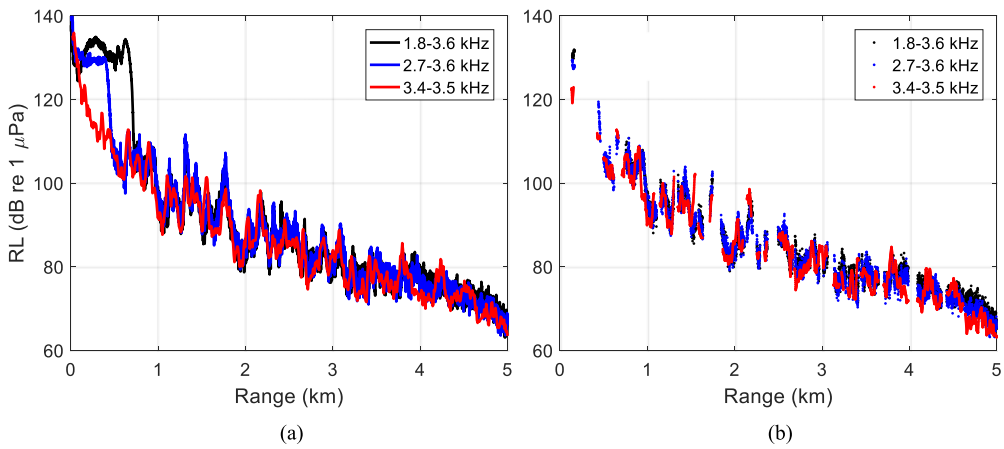

Fig. 9. Comparison of RL (a) before and (b) after biological filtering using waveforms of 1.8–3.6-, 2.7–3.6-, and 3.4–3.5-kHz LFM along 129° bearing. The frequency-dependent beam pattern effect has been accounted for, as detailed in part E of the Appendix.

B. Category I: Bottom Reverberation With Low Sea State

Two types of signals are used to study bottom-dominated reverberation (category I). The first type includes the tonal signals at 1.9, 2.7, and 3.5 kHz, and the other type includes wideband signals with varying bandwidths and center frequencies. Both types of signals were transmitted sequentially as part of the repeated eight waveform sequences. The RL recorded during local time 05:30–06:30 on April 24 (as shown in Fig. 9) is presented in Fig. 10(a)–(c), when the biological activity was low.

To study the frequency dependence of RL, Fig. 10(a) and (b) can be jointly used, representing comparisons of signals at the 1.9-, 2.7-, and 3.5-kHz center frequencies with bandwidths of 1 and 100 Hz. Both comparisons show very consistent levels and little frequency dependence for ranges less than 2 km. In the range of 2–4 km, the RL at 1.9 kHz has a higher level than the other two frequencies. The RLs at 2.7 and 3.5 kHz are consistently observed throughout the experiment to have similar levels at all ranges. Note that the elevated RL at 1.9 kHz or 1.9–2.0 kHz in the 2–4-km range may indicate this part of the data is biologically contaminated. In this case, using the 2.7–3.6-kHz signal for biological filtering may not be applicable.

The RL from the five wideband signals are compared in Fig. 10(c) with varying center frequencies and bandwidths. No frequency dependence is observed in the wideband signals. In addition, the comparison indicates that there is no bandwidth dependence among the five waveforms. The similar fluctuation patterns observed in signals of all bandwidths will be demonstrated to correlate with bottom bathymetry (see Section V).

After identification of the category I data, it was found that the variation of the RL fluctuation level related to the storm event, as shown in Fig. 7, was still present. Fig. 11 shows a compilation of category I data after biological filtering collected before (April 23–29) and after the storm (May 9–17). The striking difference between the two groups of data is the reduction in the high RL fluctuations by approximately a factor of two (in decibels) after the storm. The peak-to-trough fluctuation reduces from 20 dB before the storm to 10 dB after the storm. Interestingly, the trough regions of the RL fluctuation remain the same for both cases. In addition, as will be established in Section V, the RL fluctuation correlates with bottom bathymetry for both before and after storm data. Specifically, the high RL correlates with the swale part of the bottom while the low RL correlates to the ridge part of the seabed. Therefore, the difference in Fig. 11 indicates the scattering from the swale region has been reduced while the scattering from the ridge areas of the bottom remains constant throughout the experiment.

This significant difference in RL fluctuation influences the choice of data to use for initial data/model comparison. Since most of the environmental measurements, including seabed roughness, sound speed and attenuation, and back SS, were carried out after May 17, it is proposed here to start with data taken on May 9–17. The after storm category I data are shown in Fig. 12 using two waveforms: 2.7–3.6 LFM and 3.5 kHz tonal.

C. Category II: Reverberation With Higher Sea States

One of the major scientific goals of TREX13 is to study the effect of the sea surface conditions (roughness) on bottom reverberation at midfrequencies. For that purpose, the length of the experiment was chosen to increase the probability of collecting reverberation data, when the sea surface conditions varied from calm to rough. The sea surface conditions during TREX13 were recorded [20] using two Datawell DWR-G4 buoys, which provided estimates of the directional wave spectrum every 0.5 h. Using the buoy data, two aspects of the rough surface impact on RL are examined here: 1) surface RMS height dependence and 2) angular dependence, i.e., the dependence on relative surface wave and acoustic wave propagation directions. The surface wave propagation direction is defined as the energy weighted mean direction from which the waves propagate [25], [29]. In this section, three data sets are used to examine the rough sea surface effects on RL: one taken under a relatively calm sea during local time 05:30–06:30 on April 24 and the other two under rougher seas with different RMS surface heights and surface wave propagation directions.

The two rough sea surface conditions occurred during local times of 05:49–06:43 on May 1 and 23:48–00:36$^{(+1D)}$ on May 7. On May 1, the RMS height was approximately 0.13 m and the dominant surface wave component propagated along a bearing

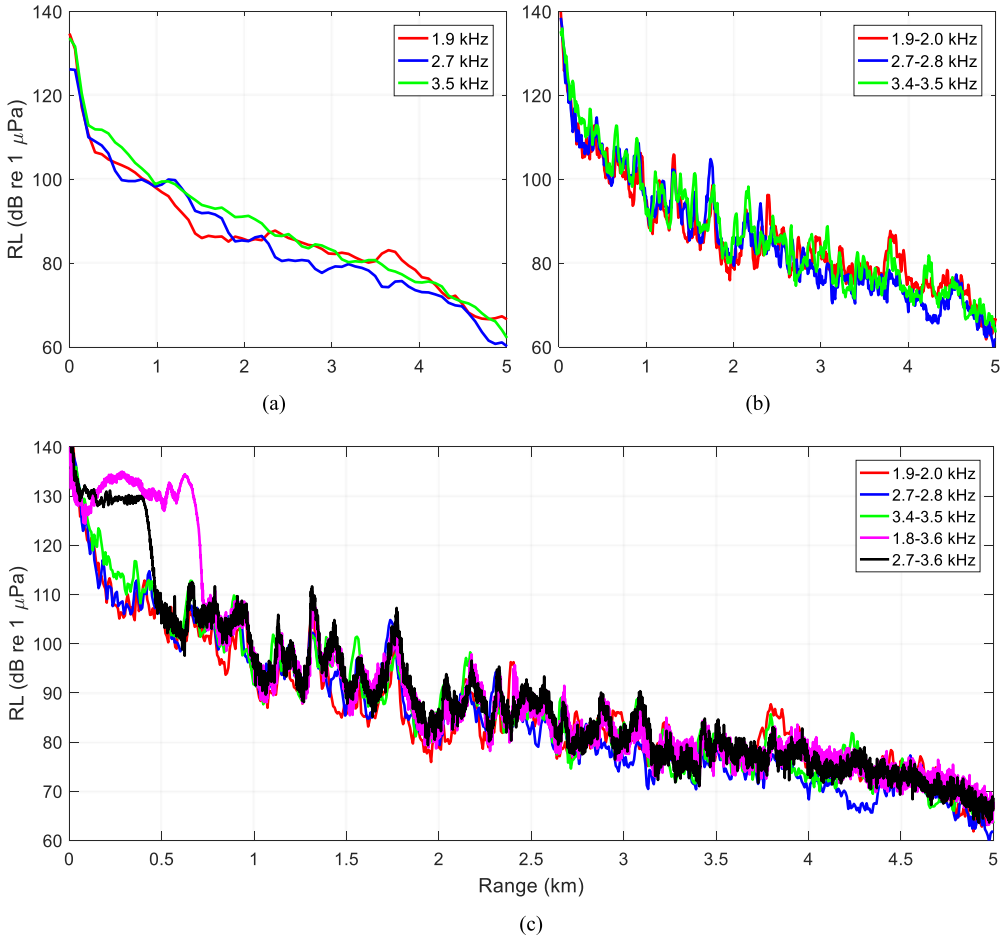

Fig. 10. RL dependence on frequency and bandwidth: (a) three sinusoidal signals at 1.9, 2.7, and 3.5 kHz; (b) three signals with 100-Hz bandwidth, 1.9–2.0, 2.7–2.8, and 3.4–3.5 kHz; (c) five signals of 100-, 900-, and 1800-Hz bandwidths, 1.9–2.0, 2.7–2.8, 3.4–3.5, 1.8–3.6, and 2.7–3.6 kHz. The data were collected on April 24, local time 05:30–06:30 along 129° bearing. The frequency-dependent beam pattern effect has been accounted for, as detailed in part E of the Appendix.

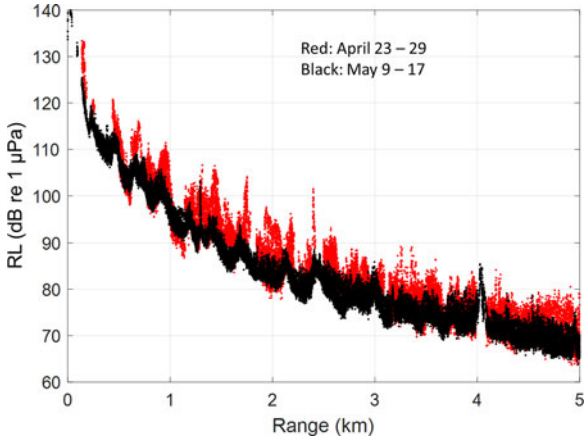

Fig. 11. Category I data before (red, 50 pings) and after storm (black, 70 pings) using the 2.7–3.6-kHz LFM signal along 129° bearing after applying biological filter.

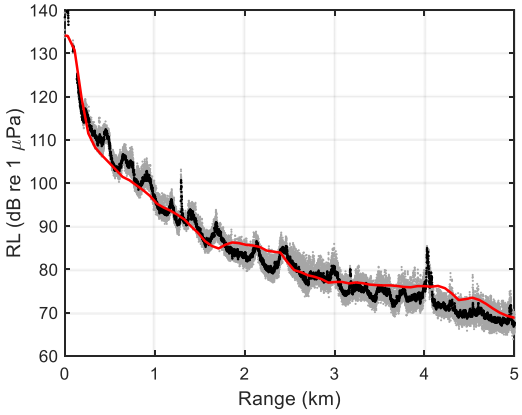

Fig. 12. Representative, after storm, category I data from the 2.7–3.6-LFM signal (gray 70 pings) and its mean (black) and mean of the 3.5-kHz tonal signal (red, 98 pings) along 129° bearing.

of 155°; whereas on May 7, the RMS height was approximately 0.25 m along a bearing of 260°. Focusing on RL along 129° in the middle of the main reverberation track, the acoustic and surface wave propagation paths are close to parallel on May 1 and in between parallel and perpendicular on May 7.

To examine the effects of the rough sea surface when the surface waves are propagating nearly parallel to the acoustic propagation direction, the RL measured on May 1 are compared to the calm sea data in Fig. 13. In this comparison 1-s tonal signals at 1.9, 2.7, and 3.5 kHz are used and all RLs displayed

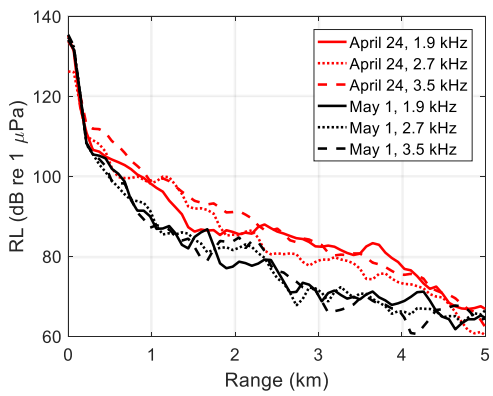

Fig. 13. Comparison of RL along 129° bearing under relatively calm (red, April 24) and rough surface conditions (black, May 1) using three tonal signals. The frequency-dependent beam pattern effect has been accounted for, as detailed in part E of the Appendix, for all waveforms.

in Fig. 13 are above ambient noise levels by at least 6 dB. The low spatial resolution of the tonal signals provides spatially averaged RL and the RL fluctuations are partially smoothed out. As shown in Fig. 13, the rough sea surface has a pronounced effect on the RL for the three tonal signals, producing an RL reduction of about 10 dB at 3 km. This reduction shows very little frequency dependence in the frequency band 1.9–3.5 kHz.

Due to scattering losses from the rough sea surface, one might anticipate an even greater RL reduction as the RMS height increases. To test this hypothesis, the RLs for the 3.5-kHz tonal signal are first compared for the low and the two rough sea states [see Fig. 14(a)]. The low sea state case has the highest RL as anticipated but the reduction in RL for the other two rough cases is not proportional to surface RMS heights. The RL fluctuation with the 0.13-m RMS height case shows a similar, if not slightly higher reduction than for the rougher 0.25-m case. This is hypothesized to be related to the effect of the surface wave propagation direction relative to the reverberation path, since for the lower RMS case, the surface wave propagates more parallel to the acoustic path (a 26° difference); whereas for the higher RMS case, the surface wave propagates neither parallel nor perpendicular to the acoustic path (a 131° difference). This paper focuses on reverberation data along the main reverberation track but RL in other directions can later be investigated to test the hypothesis and provide RL angular variation quantitatively for modeling purposes.

The RL for the 2.7–3.6-kHz LFM signal are also compared for the low and the two rough sea states in Fig. 14(b). The wideband RL show a similar dependence on the sea state as the tonal signal [see Fig. 14(a)] but with different fluctuation levels among the three cases, especially between the two rough cases on May 1 and May 7. On May 1, the last day before the storm, the fluctuation level is slightly reduced from the low sea state case. However, on May 7, the RL fluctuation diminishes significantly. The RL fluctuation level then recovers in about one and half days to about half (in decibel) of the low sea state case and remains at that level until the end of the experiment. This variation in RL fluctuation has also been confirmed using data from the ITC5485/line array. As mentioned earlier, the ITC5485/line array was fixed in location throughout the experiment and recorded the same variation in fluctuation level. Therefore, the variation in RL fluctuation level is not due to the change of geometry but rather changes in the environment, including the rough sea surface conditions on May 7 and environmental conditions during the storm that may have led to changes in sediment properties after the storm relative to those before the storm.

D. Category III Data: Reverberation That Includes Significant Biological Contributions

Biological activity is often observed in reverberation data and the beamformed RL provides a unique way to study biological activities in range, bearing, and time [30], [31]. During the experiment, a variation in RL associated with intensive biological activity was observed to increase immediately after dusk (∼20:30 local time) and disappear after dawn (∼05:00 local time). In this section, 12-h continuously recorded RL data beamformed over the southeast quarter (90°–180° bearing) are used to present the nightly evolution of biological signatures. Data presented here were recorded on April 30, 19:48–07:42$^{(+1D)}$ local time, using the 2.7–3.6-kHz signal. The interval between pings was 6 min, resulting in 10 pings per hour. These 10 pings are used to obtain an hourly averaged 2-D beamformed RL in the bearing range of 90°–180°. The 12 h of data are summarized in Fig. 15 with each panel representing 1 h averaged RL. To make it easier to compare the data collected at different times, the same general trend and SL have been removed so that the levels represent RL fluctuation in decibels.

These 12-h-averaged RLs show the progression of the biological signature in range, bearing, and time. In this data set, the biological activity starts to build up from 19:48; is the most intensive at 20:48; and disappears almost completely shortly after dawn (05:48–06:42). Biological activity is initially concentrated in the south of the box, covering an area about 4 × 6 km, producing a 20-dB increase in RL. Over time, the biological returns vary in both spatial coverage and level. One example is the area highlighted in the 20:48–21:42 panel. Over the course of the following 3 h, the biological returns in the boxed area are reduced in both spatial coverage and level. Then they increase for the next hour but eventually disappear after three more hours.

Another interesting feature, which potentially indicates a biological migration path, can be identified from 00:48–05:42 with the feature highlighted for the time period of 00:48–01:42. The highlighted feature is first spread evenly over 4 km at about 20° in bearing. The feature then moves toward the RAS location and congregates. The congregation then changes from hour to hour until it finally disappears after 6 h. This 12-h progression of RL data represents the typical nightly pattern of biological activities at the TREX13 site, i.e., biological activity increases after dusk and disappears after dawn. This is also why the majority of the category I data comes from the shortly-after-dawn period.

Traditional biological monitoring techniques are usually downward looking. The echogram, the image of the backscattered intensity map, is used to extract biological information as a function of range and depth [32]. As demonstrated by [31], the

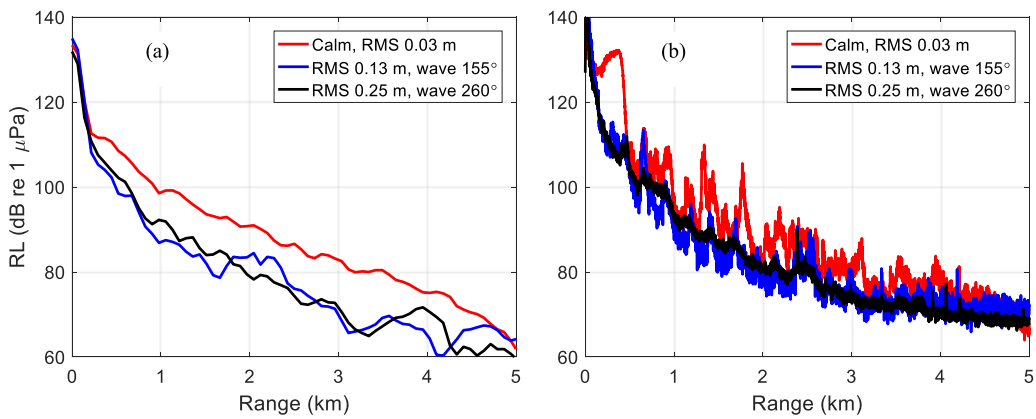

Fig. 14. Comparison of RL along 129° bearing under relatively calm and two rough surface conditions: One with 0.13-m RMS height and mean wave direction 155° (May 1); and the other with 0.25-m RMS height and mean wave direction 260° (May 7) for (a) 3.5-kHz tonal and (b) 2.7–3.6-kHz LFM signals. The beam pattern widening effect has been accounted for, as detailed in part E of the Appendix, for the three geometries.

technique presented here using the triplet beamformed RL data provides a different way to study biologics. The most notable advantage is the simultaneous view over angle and range. In addition, the RAS is stationary throughout the experiment. By examining all the RL data over 360°, especially the data taken throughout the night, rich information about biologics during TREX13 can be extracted to understand biological activity at the site.

V. Correlation Between Deterministic RL Fluctuations and Bathymetry

The RL fluctuations versus range were consistently observed throughout TREX13, and the fluctuations were found not to be random in nature. In fact, they are present in all waveforms with different center frequencies. In this section, analysis is carried out to determine the potential source of the RL fluctuation. The RL fluctuations are correlated with both bathymetry, where its corrugation shows a similar spatial variation as RL, and acoustic backscatter intensity data at 400 kHz, which can be regarded as a representation of varying surficial bottom geophysical properties. The correlation analysis demonstrates that RL fluctuations correlate more strongly with bathymetry than with the 400-kHz backscatter intensity. The analysis is extended beyond the main reverberation track to a bearing range of 109°–149° to confirm the generality of the correlation to a wider area.

To correlate RL with bathymetry or backscatter data, the three quantities are normalized in a way to best present their individual variation with range for the correlation analysis. Specifically, bathymetry data have its overall mean removed with the result representing absolute depth fluctuation in meters, roughly in the range of –0.5 to 0.5 m. The idea is to normalize both backscatter and RL data in such a way that their oscillation amplitudes fall in the same range as bathymetric fluctuation for better comparison. Therefore, the overall means were first removed from RL and backscatter data and then their maximum peak-to-trough differences in the range of 500–3000 m were normalized to unity. The normalized fluctuation results for RL, bathymetry, and backscatter data are shown in Fig. 16 with comparison of the RL to 1) bathymetry and 2) 400-kHz backscatter intensity along the main reverberation track. Note that in Fig. 16(a), the bathymetric fluctuation has been inverted, i.e., the positive values correspond to deeper valleys and negative values correspond to shallower regions. There is a clear correlation between RL and bathymetry with high RL occurring at the valley regions of the bathymetry. In comparison, the backscatter intensity fluctuation measured at 400 kHz is shown in Fig. 16(b). There is a regular saw-tooth pattern in backscatter intensity fluctuation as it goes over the sand ridges and swales. The sharp drop-offs correspond to the transitions from sand ridges to narrow mud strips that are approximately 10 m wide in range [22]. For the first three kilometers, RL and bathymetry in Fig. 16(a) have a correlation of 75% (correlation coefficient of 0.75) while in Fig. 16(b) the correlation with backscatter is 39%. These correlations are independent of sea states since both category I and II data correlate with bathymetry in the same way.

The correlation analysis is extended to a 40° wide wedge to see whether the correlations are independent of bearing. To give an overall view of how well the RL and bathymetric fluctuations correlate, the bathymetry fluctuation contours are overlaid on the RL fluctuations in Fig. 17. Two data sets, from May 1 and May 16, are used, where the May 1 data belong to category II with rough surface conditions. Both panels are rotated with the horizontal representing the 129° bearing. Note, data with biological impact were whitened out and data removal percentiles are 9% and 2%, respectively. In addition, only the positive contours, i.e., the swales or valleys in the bathymetry, are plotted to help visually identify the correlation between RL and bathymetric fluctuations. As shown in both data sets, the high RL almost invariably coincides with the contour lines, i.e., the high RL falls in the swale region of the bottom. This fluctuation pattern persists regardless of the differences in 1) sea surface roughness (May 1 rough versus May 16 calm seas) and 2) the times the two data sets were taken (before and after the storm).

For the bearing range of 109°–149°, the cross correlation coefficients are computed and overlaid on the bathymetry fluctuation in Fig. 18. The comparison is again rotated with the horizontal representing the 129° bearing. Within this 40°, the

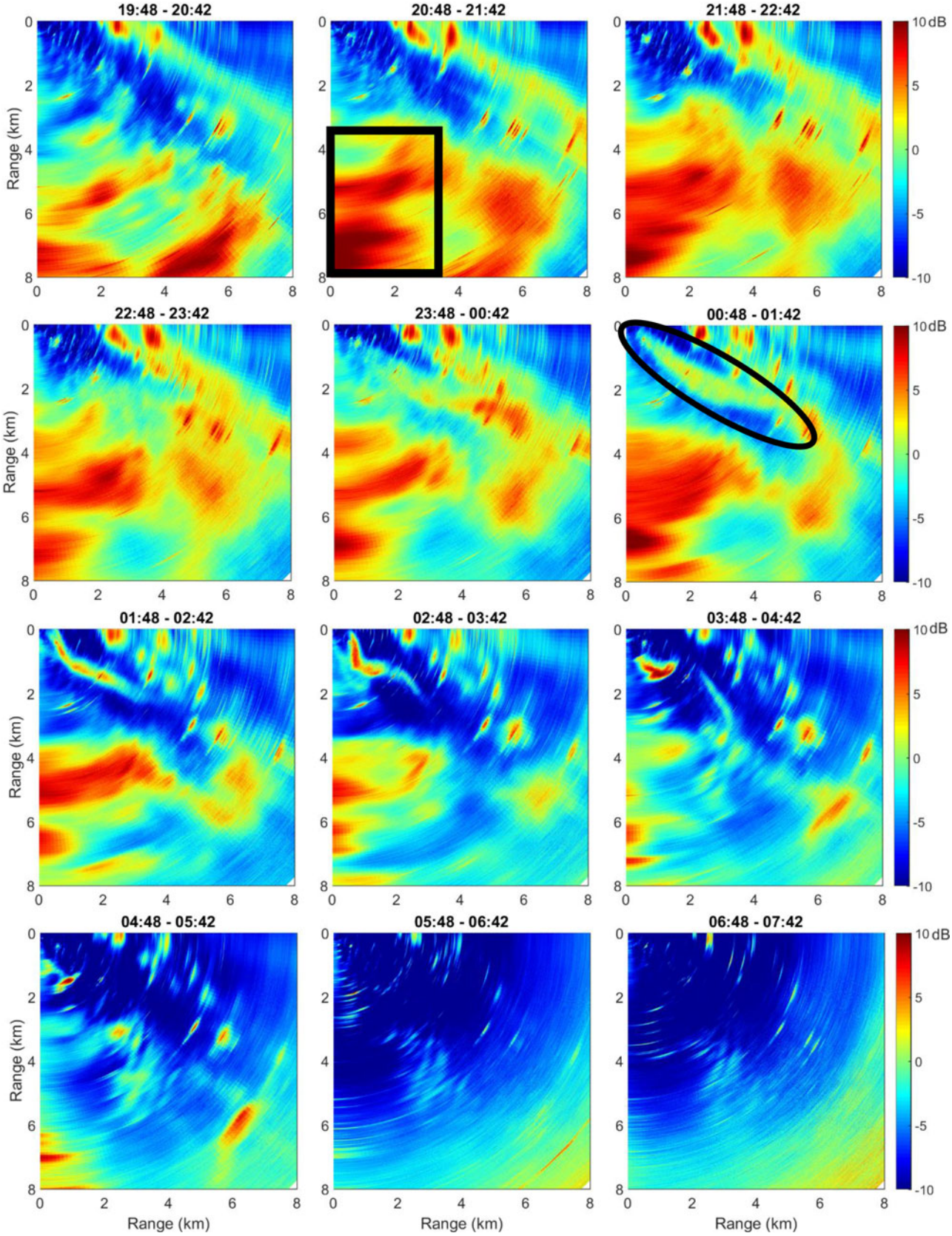

Fig. 15. Time-dependent RL showing biological activity observed on April 30 using LFM 2.7–3.6-kHz LFM over the 90° southeast quadrant over 12 h. Clockwise from top left panel, each panel represents 1-h averaged detrended RL from local time 19:48–07:42$^{(+1D)}$. A general trend of $t^{-3.4}$ has been removed from all beams.

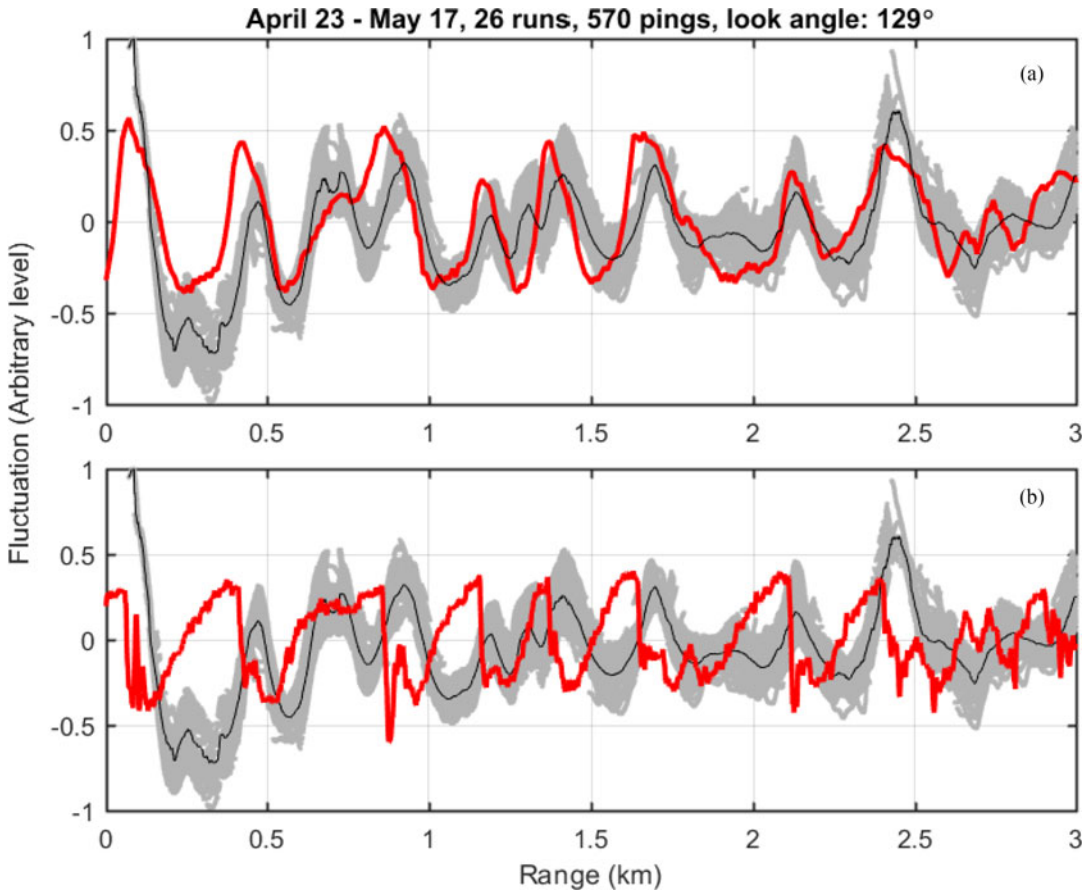

Fig. 16. Comparison of RL fluctuation with (a) bathymetry and (b) 400-kHz backscatter intensity along the main reverberation track. Gray: normalized RL fluctuation; black: overall mean of RL fluctuation; and red: (a) bathymetric and (b) high-frequency backscatter intensity fluctuation. (Note, for bathymetric fluctuations, positive number means deeper water depth and *vice versa*.)

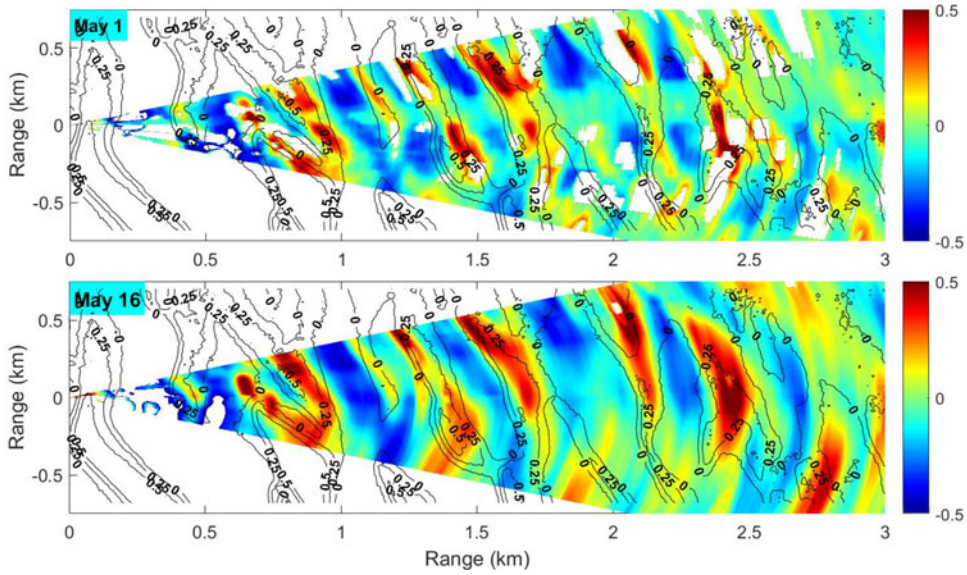

Fig. 17. Comparison of RL and bathymetric fluctuations over 40° for two data sets on May 1 (top) and May 16 (bottom). Data with biological impact were whited out and data removal are 9% and 2%, respectively. Colorbar: normalized RL fluctuation level; contours: bathymetric fluctuation contour with only the positive part shown, i.e., the swales or deeper portion of the bathymetry.

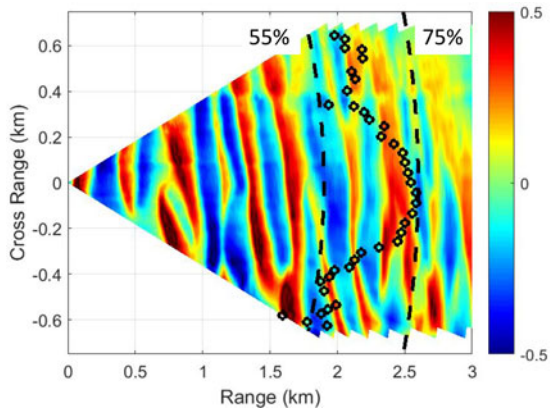

Fig. 18. Cross correlation coefficients (black circles) between RL and the bathymetric fluctuations at each angle superimposed on the bathymetric fluctuation color plot. The two dashed lines indicate cross correlation coefficients of 55% and 75%, respectively. Colorbar: bathymetric fluctuations in meters.

correlation level ranges from 55% to 75%, with the highest correlation centered near the center of the main reverberation track. This quick dropoff in correlation for bearings beyond 135° is potentially due to the more complicated bottom structures to the southeast direction.

VI. Target Echo

There are a number of targets within the TREX13 field of view that allow echo analysis, and these targets include the PAT, the vertical line arrays deployed along the main reverberation track, and the ship wrecks and bridge sections along the clutter track. Among them, the PAT is the most confined in space and will be used here to present the characteristics of target return in response to varying environmental conditions. The PAT is a 15-m-long 3″ diameter air-filled hose, deployed vertically in the water column, starting 2 m above the bottom [33]. It was deployed at 30.049° N 85.654° W, approximately 2.8 km from the *R/V Sharp* from May 2 to May 14.

Two aspects of the PAT echo are studied: 1) echo SNR, and 2) echo arrival time in response to environmental changes including sea surface conditions and water column properties. Results shown here are based on data taken from May 8–14 using the 1.8–3.6-kHz LFM signal. The data gaps in Figs. 19 and 20 are due to a lack of transmissions. In Fig. 19(a), the echo SNR is defined as the difference between the peak echo return and the background RL, which is the mean RL within a 0.1-s time window immediately before the echo. The surface RMS height is also plotted for comparison. Here, target echo SNR on May 8, May 9, and May 10 (Universal Time Coordinated (UTC)) are discussed.

On May 8, surface RMS height started high at 0.25 m and the echo SNR is a mere 5 dB. As the rough surface condition subsides, the echo SNR increases to 15 dB [see Fig. 19(a)]. This is also demonstrated in the target echo data shown in Fig. 19(b), with the two curves representing the high (0.25-m RMS height) and low (0.15 m RMS height) surface roughness conditions of the data on May 8. The background RL is similar at both times but the echo signal differs by about 11 dB. This suggests the sensitivity of the target echo to surface roughness. With a rough surface, forward scattering will redistribute acoustic energy to a range of angles and therefore result in a loss of coherence, hence the reduced SNR.

In addition to surface conditions, the echo SNR can also be influenced by biological activity and shipping noise. For example, the data on May 9 [see Fig. 19(c)] were affected by frequent shipping noise. The shipping noise caused a 15-dB, occasionally as high as 25-dB, variation in background level (RL + noise), whereas the echo signal level remained relatively stable. The combination of the two factors results in the 15-dB spread in hose echo SNR.

A well-defined arch, as shown in Fig. 20(a), pattern is observed in echo SNR in a span of 10 h on May 10. The echo returns (not shown here) are well-defined, with stable background RL and no observable noise contamination. This gradual change in SNR is assumed to be a response to a sound speed change in the water column. While continuous sound-speed profile data were not available, the water column temperature was recorded as a function of time by a thermistor chain mounted on VLA #2. In Fig. 20(a), the echo SNR with RMS heights is shown once more to compare with Fig. 20(b), the temperature data in Celsius for the time period of May 8–12. Interestingly, the arch shape of the echo SNR fits well with a similar pattern in the temperature data. Focusing on the 10–12-m depth, the water column appears to experience a process of cooling and warming, with the maximum cooling coinciding with the maximum echo SNR.

The same data are used to find the echo arrival time shown in Fig. 20(c). Echo arrival time here is defined as the time at the peak of the target echo and represents the two-way travel time to and from the target. Two interesting features in Fig. 20(c) are worth discussing. One is the large fluctuation in echo arrival time on May 8, which was a day with rough sea surface conditions [see Fig. 20(a)]. The spread in arrival time is about 15 ms, corresponding to a spatial variation of about 11.5 m using 1526 m/s for the sound speed in water. This variation is potentially due to 1) the motion of the PAT and 2) scattering from the rough sea surface, with the latter likely being the dominant cause of the variation for two reasons. One is that, given the dimension of the PAT, it is unlikely that its motion can account for the 11.5-m spatial variation. The second reason is that since the arrival time is defined at the peak of the echo, scattering from the rough sea surface tends to redistribute energy to higher grazing angles and results in the delay of the signal peak, consistent with Fig. 20(c).

The other interesting feature is the general trend toward shorter echo arrival time over the course of four days, May 8–12. Excluding data with rough surface conditions, the arrival times of the three data sets (May 9–12) are tightly bounded within each data set but show an overall reduction of 5 ms in arrival time. On May 8, sound-speed profiles show that the average water sound speed is 1526 m/s. Given the distance between PAT and RAS (2.8 km), the 5-ms reduction in arrival time would require the sound speed to increase from 1526 to 1530 m/s. The temperature data, as shown in Fig. 20(b), clearly show an overall warming trend from May 8–11. The increase in temperature is

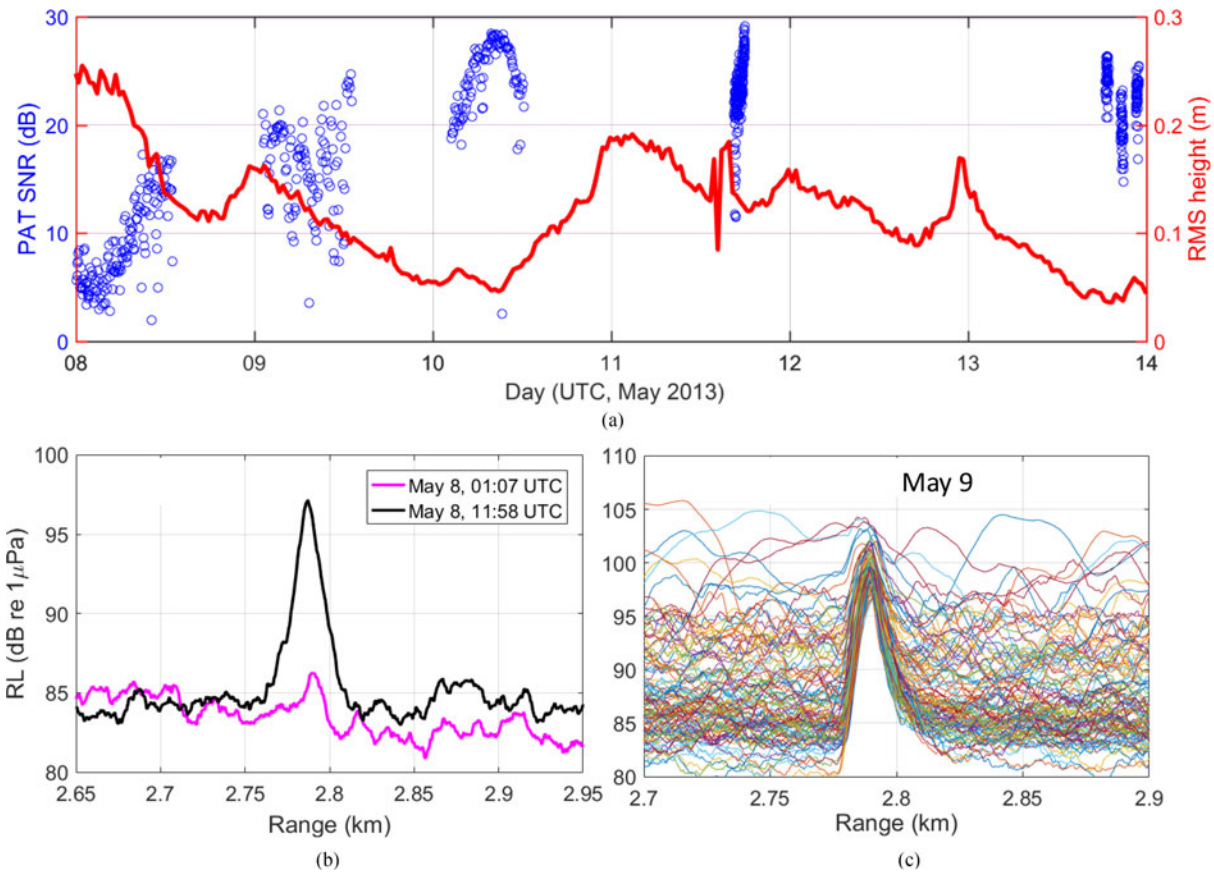

Fig. 19. (a) Comparison between PAT target echo signal-to-background level and sea surface RMS height using the 1.8–3.6-kHz signal. (b) PAT target echo returns on May 8 with magenta and black curves representing RMS height of 0.24 and 0.15 m. (c) PAT target echo returns on May 9 with different levels of shipping noise.

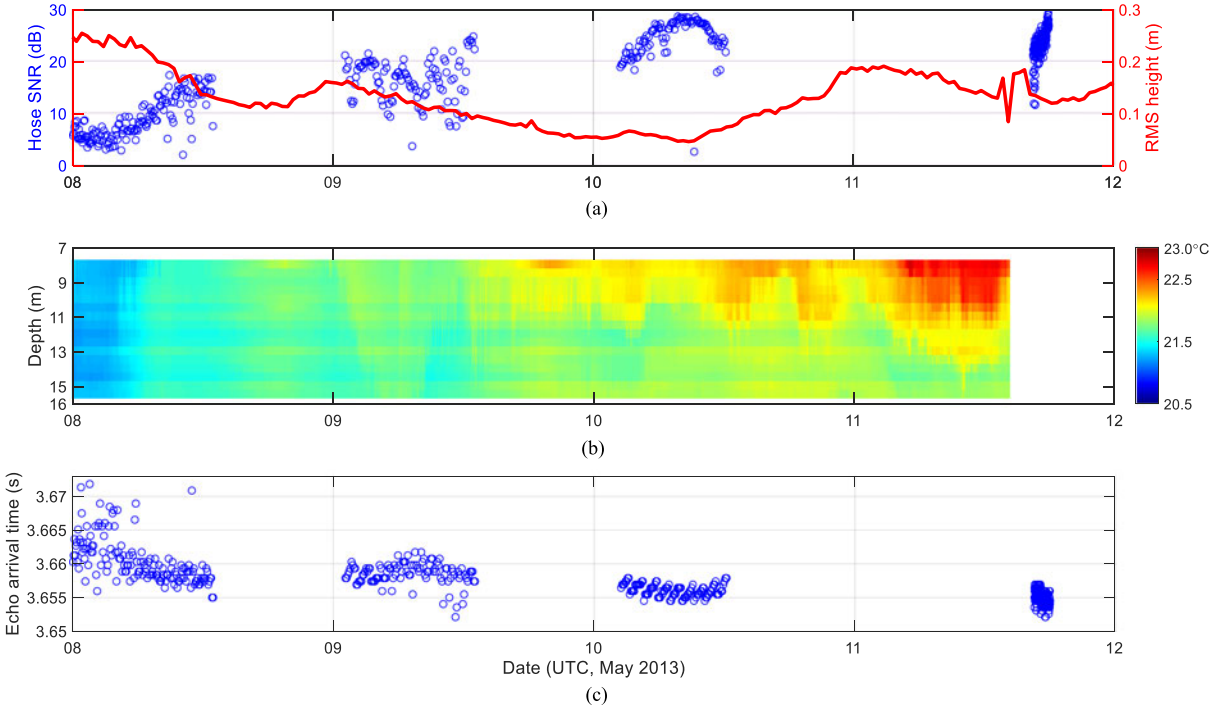

Fig. 20. (a) Comparison between PAT target echo signal-to-background level and sea surface RMS height using the 1.8–3.6-kHz signal between May 8–12, 2013. (b) Color plot of water column temperature using the thermistor chain data on VLA #2. (c) PAT target echo arrival time using the 1.8–3.6-kHz signal.

about 1°, which would provide a 4-m/s increase in sound speed to support the echo arrival time reduction.

This section presented echoes from the simplest target at TREX13 and how the target echo responded to environmental conditions including surface roughness and water column properties. Compared to the reverberation data, the target echo is more sensitive to environmental conditions. One of the goals of this experiment is to understand what environmental parameters are most important to measure to accurately predict sonar performance. The analysis of target echo response to environmental conditions performed here indicates that reverberation and target response modeling at midfrequencies require different kinds of information.

VII. Supporting Environmental Measurements and Guidance for Modeling

During TREX13, extensive environmental measurements were carried out to support detailed data/model comparisons along the main reverberation track. The environmental measurements that are important to model reverberation include sea surface and bottom roughness spectra, bottom geoacoustic properties, and sediment volume heterogeneity. In this section, general information about these measurements is given, organized by their utility in addressing the major observations in reverberation. Details of the measurements and resulting parameter values are given in references.

A. Measurements of Bottom Properties for Understanding Category I RL Fluctuations

The most pronounced feature in bottom-dominated RL is its deterministic fluctuation, which may be due to bathymetry, range-dependent interface roughness, geoacoustic properties, sediment volume heterogeneity, or a combination of multiple mechanisms. To understand RL and its fluctuation, extensive environmental measurements of both surficial and subbottom properties were carried out during TREX13. Environmental data representing surficial properties include fine-scale bathymetry, backscatter intensity at 400 kHz [21], and sediment roughness power spectra [22]. Subbottom measurements include chirp surveys and cores [23], sediment sound speed and attenuation [24], and cone penetrometer measurements [34]. The single path backscatter [19] measures the combined effects of both surficial and subbottom properties of the seabed.

In Section V, RL fluctuations have been shown to correlate with bathymetry. Preliminary numerical calculations, however, demonstrate a contradiction, i.e., high RL is expected to come from the ridges and low RL from the swales, if bathymetric variation is the only range-dependent parameter. Sediment interface roughness spectra were measured using the seafloor laser scanner (SLS) at 14 sites to capture the roughness variation along the main reverberation track. It has been possible to extend the spectral parameters over the entire main reverberation track by an observed correlation between the point measurements from SLS and the backscatter intensity data at 400 kHz with 10-m spacing. In the frequency band of 2–4 kHz, the predicted spectral strength indicates about 3–4-dB variation in roughness along the track [22].

For subbottom properties, significant volume scattering was measured using different techniques, including the single path backscatter, bottom/buried object scanning sonar (BOSS), and subbottom chirp surveys. The single path backscatter experiment obtained bottom backscatter strength in a grazing angle range of 20°–60° using the Bottom Backscatter Sonar (BBS, [19]). BBS consists of a omni-directional source (ITC1007) and a receiver (ITC1032) mounted on a short bracket with 0.35-m spacing. Results show that backscatter strength over the sandy region is dominated by roughness while over the muddy area, volume heterogeneity dominates. Backscatter strength is extended through modeling to low grazing angles. At 10°, the back SS is about 10 dB higher in swale areas than on the ridges.

Volume backscatter intensity was measured using the BOSS as well [19]. The BOSS is a downward-looking subbottom imaging sonar system designed to detect buried objects. It was deployed by the Naval Surface Warfare Center on June 23–25, 2013. BOSS has two 20-channel hydrophone arrays on two extended wings of an autonomous underwater vehicle. BOSS allows scattering voxels of size 10 cm $\times$ 10 cm $\times$ 10 cm to be obtained. Broadband signals (3–20 kHz) were transmitted along two 5-km tracks parallel to the main reverberation track with 15-m separation. Although uncalibrated in absolute level, the variation in volume backscatter intensity is about 6 dB from the sand ridges to the swale valleys. In addition, subbottom chirp profiling and free-falling cone penetrometer data, collected by Defense Research and Development Canada (DRDC), Ottawa, ON, Canada, are also available along the main reverberation track [34].

Finally, sediment sound speed and attenuation were measured at five sites along the main reverberation track, representing sandy, muddy, and mixture sediment types [24]. Sediment sound speed changes from 1580 to 1660 m/s and attenuation changes from 0.5 to 1.3 dB/m between the soft muddy and coarse sandy sites at 3 kHz. In addition, the sound-speed dispersion is about 3% at a coarse sandy site and about 1% at the muddy site.

Combining all measurements, a range-dependent geoacoustic landscape can be determined to support detailed data/model comparison.

B. Monitoring Sediment Property Changes Due to a Storm

Another interesting observation in RL data is the difference in category I, bottom dominated reverberation at low sea state before and after the storm. As shown in Fig. 11, the high RL fluctuation reduces from 20 to 10 dB before and after the storm, while RL from the sand ridges remains about the same. In addition, data taken on May 7, which is close to the end of the storm but still with a rough sea, show that the RL fluctuations almost completely diminished. It took about 1.5 days for the fluctuations to reestablish to about half of the level before the storm and then persist till the end of the experiment.

Environmental data were recorded on two fixed quadpods, with one near the main reverberation track at 19-m water depth and the other inshore at 7.5-m water depth, which may indicate a mechanism responsible for the variation in fluctuation level.

Each quadpod has instruments that measured surface directional roughness spectra, current direction and speed, ripple formation, sediment suspension, and the water conductivity, temperature, and density [26]. Both quadpods were deployed from April 20 to May 23. During the storm event on May 6, a ripple field was observed to form with crests close to parallel to the main reverberation track that decayed in about two days. In addition, the modeling predicts that up to 10 cm of sand could have been transported and redeposited by the storm [26]. This deposited sand could have produced a reduction in the sound penetration into the sediment and hence decrease the amount of volume scattering.

C. Forward Loss Model Due to Directional Surface Wave Field

The observation of the rough sea surface impact on midfrequency reverberation was an important goal of TREX13. With the help of the directional surface wave spectra from the wave buoys and the beamforming capability of the triplet array, one can study the impact of the rough sea surface on RL as functions of both RMS height and the angle between the acoustic wave and the surface wave propagation directions. TREX13 data show RL dependence on both. Model development is currently ongoing to account for these effects.

D. Oceanographic Influence on Target Echo

In Section VI, the sensitivity of a target echo to changing environmental conditions was presented. The varying environmental conditions include rough sea surface and water column sound speed. Since the target echo varies with signal coherence, it will likely be more affected by environmental conditions, compared with reverberation data. To successfully model the target echo, a more complete set of environmental data is needed. Available oceanographic data include two thermistor strings on the two vertical line arrays at ranges of 2.4 and 4.2 km, ship conductivity–temperature–depth (CTD), and currents measured on the quadpod. The thermistor string data show water column warming and cooling on both small (semidiurnal) and large (several day) time scales [35].

VIII. Summary

TREX13 was carried out from April 21 to May 17 near Panama City, FL, USA. To measure reverberation, both the source and receive array were mounted above the seafloor with the array suspended horizontally between tripods. Reverberation data were taken day and night under diverse environmental conditions in the frequency band of 2–10 kHz with an emphasis on 2–4 kHz. Companion environmental data, including fine-scale bottom bathymetry, bottom roughness, sea surface roughness, sediment sound speed and attenuation, and water sound-speed profiles, were measured to support detailed data/model comparisons.

Reverberation data presented in this paper are from the toroidal ITC2015 source and the triplet array, Four Octave Receiving Array (FORA), and are match-filtered and beamformed to provide RL. Various waveforms, both narrow and wideband, are used to study the mechanisms that affect RL such as scattering from the seafloor, propagation losses, and the presence of biologics. Over the course of TREX13, RL was observed to have an overall 17-dB variation in mean level at a range of 3 km due to a combination of mechanisms. A persistent and pronounced RL fluctuation pattern out to a range of 3 km is observed, which has been established to correlate with bottom bathymetry to 75% along the main reverberation track. Specifically, the high RL comes from the swale part of the bottom, whereas the low RL comes from the sand ridges. The data also indicate that the fluctuation is due to distributed scatterers instead of to a few spatially confined scatterers. In addition, the RL fluctuation level was observed to vary over time: the peak-to-trough fluctuation was up to 20 dB before the storm (April 23–May 1), almost nonexistent right after the storm (May 7–8), and recovered to 10 dB for the rest of the experiment (May 9–17).

To achieve quantitative understanding of RL through modeling, the reverberation data have been carefully divided into three categories, which emphasize 1) bottom reverberation with low sea state; 2) bottom reverberation with higher sea state; and 3) biological impacts. Category I is defined for data where the seabed is the dominant reverberation source, with calm seas (sea surface RMS height less than 0.1 m), low ambient noise, and no apparent biological activity. Category II has the same criteria as category I except that RMS surface heights are greater than 0.1 m. Category III corresponds to data with biological signatures, i.e., features in RL that are transient in both space and time.

Category I data are used to study the characteristics of bottom dominated reverberation and its dependence on frequency, bandwidth, range, bearing, and time at the TREX13 site. Both tonal and wideband signals are used to study the frequency dependence in the band of 1.9–3.6 kHz. Little frequency dependence is observed. In addition, bandwidths of 100, 900, and 1800 Hz are compared, which show little bandwidth dependence in mean levels of RL. Signals of all bandwidths show consistent RL fluctuations with spatial scales of 200–300 m. Over a 40° bearing section, the RL fluctuation varies in range from bearing to bearing but the mean RL are consistent.

One interesting phenomenon observed in the category I data is the variation of the reverberation fluctuation levels before and after the storm. Before the storm, RL has a maximum peak-to-trough fluctuation of 20 dB, which is reduced to 10 dB after the storm. Interestingly, the reduction in RL fluctuation occurs in the RL peaks; the low RL envelope before and after the storm remains unchanged. Based on the correlation analysis, this indicates the swale part of the bottom responds differently before and after the storm; while the response from the ridge part of the seabed remains the same. This discrepancy leads to the question of what data should be used for modeling bottom-dominated reverberation. It is proposed in this paper that the data after the storm be used for initial modeling work, since most environmental measurements were carried out after the storm. Final curves of both wideband (2.7–3.6 kHz) and tonal (3.5 kHz) reverberation results are provided (see Fig. 12) for comparison with modeling for the case of bottom dominated reverberation with low sea states at the TREX13 site.

The rough sea surface has significant impact on bottom reverberation data at midfrequencies. Two representative category II data sets are presented in this paper with different sea surface conditions. The surface conditions are described by the directional surface wave buoy data, which provides 2-D spectra of the rough surface. The 2-D spectra are used to obtain RMS height and wave propagation direction. First, acoustic data between low and higher sea states have been compared. The three tonal signals at 1.9, 2.7, and 3.5 kHz show a reduction of 10 dB in RL at 3 km due to the rough surface. Little frequency dependence is observed among the three frequencies. The comparison is then done among data for one low and two higher sea states with different RMS surface heights and propagation directions. For one rough case, the RMS height is 0.13 m, with surface waves propagating parallel to the acoustic propagation direction; while the other case has an RMS height of 0.25 m, with waves propagating neither parallel nor perpendicular to acoustic propagation direction. The RL data of the three cases demonstrate there can be important effects on RL related to the propagation direction of the surface waves: The case with a lower RMS and sea surface wave propagation approximately parallel to the acoustics has a similar or slightly higher reduction in RL than the case with a higher RMS but surface wave propagation not parallel to the acoustics. This observation is significant from a modeling standpoint, especially in guiding how forward scattering should be handled.

Triplet beamformed RL provides a unique way to study the biologics for category III data. As demonstrated in the paper, the beamformed RL offers a 360° view of the biological activities over time, and allows one to study the evolution of biological signatures. One data set was used as an example, which was recorded on April 30 from local time 19:48 to 07:42 the next day. A 90° sector is shown using the hourly averaged beamformed RL. This 12-h evolution of biological signatures is representative of the nightly pattern observed during TREX13, i.e., increased biological activity starting after dusk and disappearing after dawn. For this particular data set, it caused up to a 20-dB increase in RL in some regions of the 4×6-km area examined. A possible biological migration path is observed in the 12-h progression. The quiet time after dawn is the main contributor to the category I data.

Finally, the PAT is chosen to represent the characteristics of target echoes under different environmental conditions. Two aspects of the target echo are investigated: 1) the echo SNR and 2) its arrival time. Both are observed to be sensitive to rough surface conditions. The echo SNR can drop from 20–30 dB for a low sea state to 5 dB for a sea with a RMS height of 0.25 m. The same rough surface causes the echo arrival time to have a 15-ms spread. The echo arrival time is also observed to decrease continually over a period of three days. The reduction was traced to a general warming up of the water column, which was recorded on the thermistor chains.

Appendix

During TREX13, three acoustic sources and two receive arrays were used. Specifically, the sources were the ITC2015, ITC5485, and ITC5490. The two receive arrays were a conventional horizontal line array and a triplet array. This Appendix summarizes their specifications, experimental geometries, transmitted waveforms and SLs. A discussion on the cardioid array beam pattern is included as well.

A. Sources

The ITC2015 was used as the main source for acoustic transmissions during TREX13 and acoustic transmission from the ITC2015 covers the frequency band of 1.9–8.4 kHz. As shown in Fig. 21(a), it was mounted on a pedestal 1.2 m above the seabed. It is a toroidal source, i.e., azimuthally omni-directional, with vertical beam patterns that were calibrated at the Applied Physics Laboratory, Seattle, WA, USA, between 2 and 5 kHz [36]. Vertical beam patterns were measured at four azimuth angles. Fig. 21(b) shows vertical beam pattern measured at 3 kHz with the source sitting upright as in Fig. 21(a). At 3 kHz, the main one-sided beamwidth, i.e., the angle where the beam pattern intensity decreases 3 dB relative to the peak, is 35°. The antisymmetry in the vertical, i.e., top versus bottom, is due to the mounting system at the bottom of the source.

The calibrated transmit voltage response (TVR) curve for the ITC2015 is shown in Fig. 21(c), which provides necessary information for SL estimation. In the frequency band of 2–3 kHz, the source TVR varies less than 1 dB, followed by approximately a 4-dB drop from 3–3.8 kHz. The calculation of SL for a tonal or narrowband signal, as given in part D of the Appendix, involves the addition of two components: 1) the mean-square voltage input to the source in decibels and 2) the TVR at the corresponding frequency of the transmitted signal. For wideband signals, an averaged in-band TVR is used to estimate SL.

As shown in Section III-A, the matched filter processing uses the drive voltage as replica, assuming negligible effects of the source TVR on the replica. For 100-Hz bandwidth waveforms centering at 1.95, 2.75, and 3.45 kHz, the source TVR varies 0.7, 0.2, and 0.6 dB, respectively. For wideband pulses such as the 1.8–2.7-, 2.7–3.6-, and 1.8–3.6-kHz LFM, the maximum in-band TVR variation is 2.5, 4.5, and 4.5 dB, respectively. Simulation was conducted to quantify the effect on the matched filter processing using a flat versus the real source TVR for the three wideband signals. The results (not shown here) show 1.3%, 1.5%, and 3.3% difference in peak amplitude ratio and 1.3%, 1.5%, and 4.6% in the full 3-dB width ratio between using a flat versus the real TVR for the 1.8–2.7-, 2.7–3.6-, and 1.8–3.6-kHz LFMs.

The other two sources used during TREX13 were the ITC5485 and the ITC5490, and both were directional sources. Fig. 22(a) shows the two sources assembled on one metal frame, which is about 1.2 m above the seabed. The ITC5485 consists of a series of elements and the optimum frequency band it covers is 2.5–6.5 kHz, as shown in its TVR in Fig. 22(b). At 3 kHz, its horizontal and vertical beam widths are 12° and 45°, respectively. During TREX13, the ITC5485 transmitted similar waveforms to those transmitted on the ITC2015. Data collected using these sources are not presented in this paper.

The ITC5490, the single unit above the ITC5485 in Fig. 22(a), is tuned to transmit near 9 kHz [see Fig. 22(c) for its TVR]. At

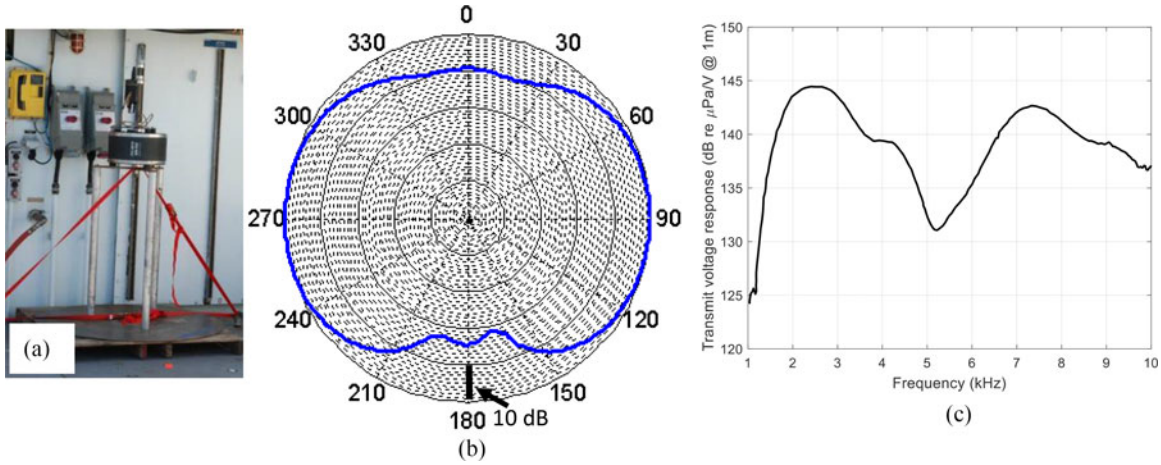

Fig. 21. (a) ITC2015 on 1.2-m-tall pedestal. (b) Calibrated vertical beam patterns at 3 kHz at one azimuthal angle with source sitting upright. (c) Calibrated ITC2015 transmit voltage response curve.

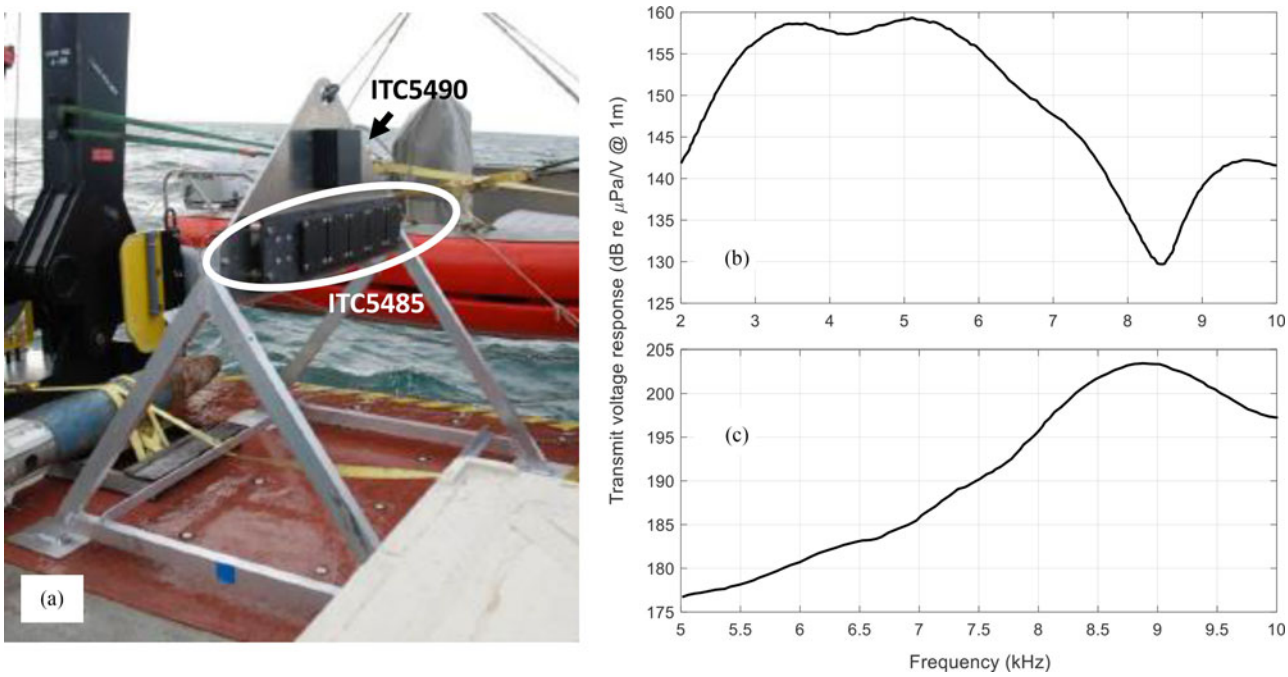

Fig. 22. (a) ITC5485 and ITC5490 on one frame and source TVR curves for (b) ITC5485 and (c) ITC5490.

9 kHz, the horizontal and vertical beam widths are 15° and 20°. During TREX13, ITC5490 transmitted one type of waveform, which is 1-s tonal signal at 9 kHz. Most of the data from ITC5490 were taken under rough sea conditions, with the goal of studying rough sea surface effects on reverberation at a higher frequency in comparison with the data presented in this paper (2–4 kHz). Data from the ITC5490 will be reported independently in the near future.

B. Receiving Arrays

Two receiving arrays were used during TREX13: one was a triplet array called Four Octave Receiving Array (FORA) [15] and the other was a conventional line array. In comparison with a conventional line array that has a single row of acoustic receivers, each acoustic element of the FORA consists of three acoustic receivers [15], which enables left/right discrimination. During TREX13, only a subsection of the FORA was usable, which has a total of 48 triplet elements with 20-cm spacing, resulting in a broadside beamwidth of 2.2° at 3.5 kHz. This beamwidth is measured between two points that are 3 dB down from the peak of the main beam. The sampling frequency of FORA is 12.5 kHz. The conventional line array, called Hangzhou Applied Acoustics Research Institute (HAARI), has 32 elements with spacing of 21.4 cm. At 3.5 kHz, the main beamwidth is 3.3° and the sampling frequency is 25 kHz.

C. TREX13 Geometries of Sources and Receiving Arrays

During TREX13, the sources and receiving arrays were paired into two independent reverberation measurement systems. The

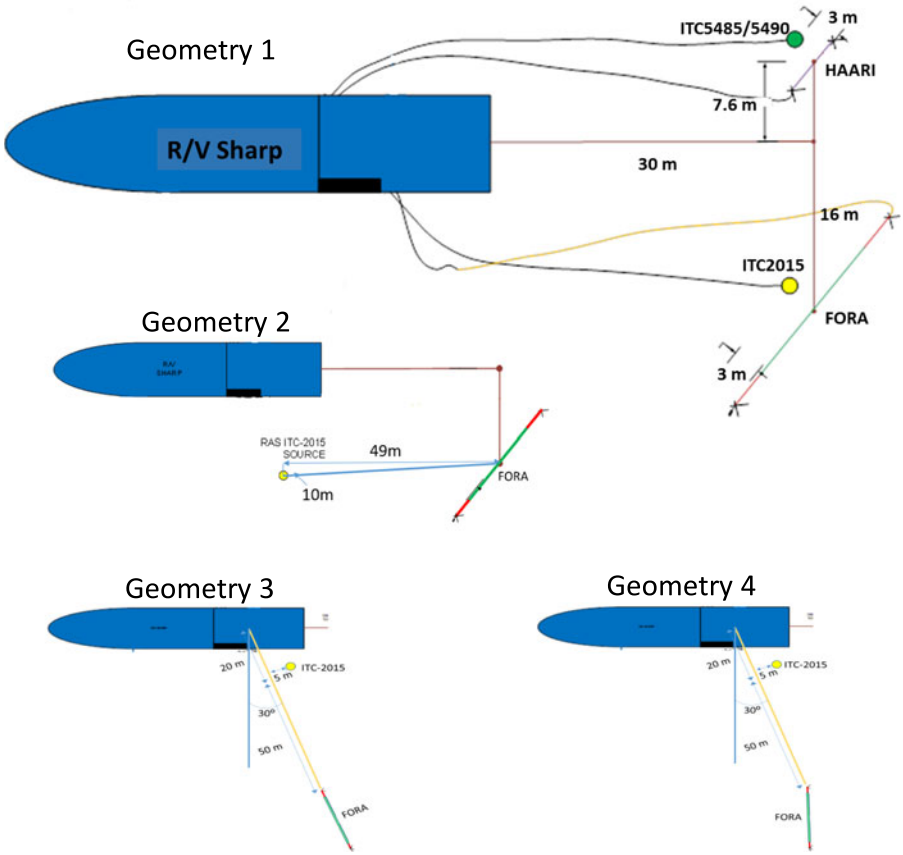

Fig. 23. Experimental geometries for the two reverberation measurement systems. ITC5485/HAARI remained at the same position throughout the experiment while ITC2015/FORA was moved three times (see Table I for all positions and array orientations).

ITC2015 and FORA pair is referred to as the RAS, which constitutes the majority of the TREX13 reverberation data and all the data presented in this paper. The ITC5485/5490 and HAARI are used as a reference system for the RAS, since their locations had remained the same throughout the TREX13. As a line array, HAARI does not have the same capability to distinguish left and right ambiguity as the FORA. However, with a directional source, the beamformed RL from ITC5485/HAARI can be compared with RAS. The beamformed RL from RAS has lower noise level than that from ITC5485/HAARI, owing to its backside rejection capability. Though treated as two independent systems, both FORA and HAARI were used to record data simultaneously, regardless of which source was being used.

Fig. 23 shows the experimental geometries for the two acoustic systems, relative to the *R/V Sharp*. The ship was in a four-point moor and lines were fixed on the bottom and measured by divers. Also with diver support, the two acoustic systems were first deployed with their broadside facing the 129° bearing, as shown in Fig. 23, geometry 1. The ITC5485/HAARI system remained at its location throughout TREX13 including the storm period, May 1–6. The RAS was repositioned three times during the experiment and a summary of the locations and orientations is given in Table I. Of the four RAS geometry positions, all were close to monostatic configuration with a maximum separation of 60 m between the source and the receiving array.

TABLE I
EXPERIMENTAL SETUP FOR RAS THROUGHOUT TREX13

Time period (local time)	GPS location ITC2015	GPS location FORA array center	FORA Heading (° re North)
1150 4/21–0900 4/26	30° 3.5862' N 85° 40.8318' W	30° 3.5856' N 85° 40.8324' W	217
1100 4/26–1500 5/1	30° 3.5808' N 85° 40.8642' W	30° 3.5856' N 85° 40.8324' W	217
1400 5/7–0815 5/8	30° 3.5850' N 85° 40.8504' W	30° 3.5562' N 85° 40.8348' W	334
0900 5/8–0730 5/17	30° 3.5850' N 85° 40.8504' W	30° 3.5550' N 85° 40.8378' W	356

D. Transmitted Waveforms and Source Levels

Various waveforms were used during TREX13 to study the dependence of reverberation on frequency, bandwidth, space (range and bearing), time, and environmental conditions. Since data presented in this paper focuses on transmissions from ITC2015, this section summarizes all waveforms and their SLs from the ITC2015.

LFM waveforms and tonal signals were transmitted, covering the frequency band of 2–10 kHz with an emphasis on 2–4 kHz. Table II lists the waveforms that were used during TREX13 using the ITC2015: LFM signals with 100-, 900-, and 1800-Hz bandwidths and tonal signals at 1.9, 2.7, and 3.5 kHz. The pulse

TABLE II
ACOUSTIC WAVEFORMS TRANSMITTED AND THEIR SOURCE LEVELS, APRIL 21–MAY 1*

Waveform type	Frequency (kHz)	Pulse length (s)	Source level (dB re 1 μPa at 1 m)
LFM	1.8–2	1	196.1
LFM	1.9–2	1	196.4
LFM	2.6–2.8	1	197.8
LFM	2.7–2.8	1	197.9
LFM	3.3–3.5	1	200.2
LFM	3.4–3.5	1	199.8
LFM	1.8–2.7	1	197.3
LFM	2.7–3.6	1	195.4
LFM	1.8–3.6	1	196.3
LFM	6.6–8.4	1	186.5
CW	1.9	1	196.1
CW	2.7	1	197.8
CW	3.5	1	199.4

*Source Levels were 1-dB Lower for May 7–17 when a Different Power Amplifier was Used

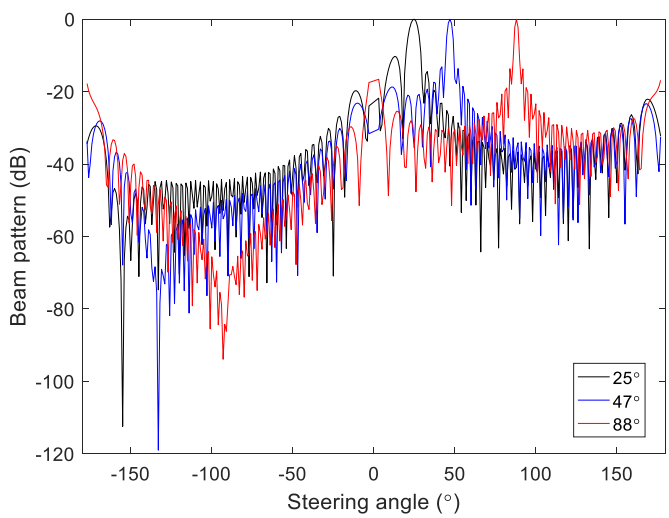

Fig. 24. Cardioid beam patterns for steering angles of 25°, 47°, and 88° at 3.5 kHz. Broadside is 90°.

lengths and SLs are listed as well. All transmitted signals had 10% Hanning window tapering at the beginning and end of the signal and recording always started 1 s before transmission to measure ambient noise. Before the storm, the acoustic transmissions consisted of repetitions of a sequence of 8 waveforms: the 1.9–2.0-, 2.7–2.8-, 3.4–3.5-, 1.8–3.6-, 2.7–3.6-, 1.9-, 2.7-, and 3.5-kHz signals. After the storm, the emphasis shifted to 1.8–2.7-, and 2.7–3.6-kHz LFMs with some coverage of other waveforms.

E. Cardioid Array Beam Pattern

In the cardioid beamforming process, beam pattern is an inherent component of the algorithm and its shape and normalization can affect absolute RL [37]. The cardioid processing in this paper is based on the work by Haralabus *et al.* [28], which prioritizes the beam pattern normalization for "back-side" rejection (see Fig. 24). Specifically, it produces a normalized peak for the main beam and a null for the ambiguous beam. This normalization scheme ensures a uniform target echo response, should the same target appear at different steering angles. However, similar to conventional beamforming, this beam pattern varies with steering angle, i.e., the main beam widens as it approaches endfire. This results in an increase of RL as the beam is steered from broadside to endfire, assuming an azimuthally uniform spatial distribution of scatterers causes reverberation. In cross-beam comparisons of RL, this effect is accounted for through the following procedure.

The RL data presented in this paper focuses on the main reverberation track, which is 88°, 25°, and 47° relative to the endfire of the FORA array due to the change of geometries (see Table I). As an example, the three corresponding beam patterns at 3.5 kHz are shown in Fig. 24. With 90° representing broadside, the widening of the main beam can be clearly observed, as the beam steers from 88° (approximately broadside) to 25° relative to endfire. The integrated intensity of each beam pattern can be calculated and their difference is due to the beam pattern variation at different steering angles. When cross-comparing RL along the main reverberation track for different geometries, the beam widening effect is taken into account. By referencing the intensity of all beams to that of the broadside, the RL should be lowered by 0.3, 0.3, 1.7, and 4.3 dB for the four geometries, respectively, for cross-comparison purpose. Note, for target echo, there is no need to account for the array beam pattern among different geometries.

In addition to the steering angle dependence, the cardioid beam pattern varies with frequency as well. In the study of the frequency dependence of RL at 1.9, 2.7, and 3.5 kHz, a similar procedure was carried out to account for the intensity difference among the three frequencies due to this beam pattern variation. In short, the main beam, with peak normalized to unity, becomes narrower from low to high frequency and therefore, results in a decrease in RL, given the same assumption of an azimuthally uniform spatial distribution of scatterers. When investigating the frequency dependence, the effect of beam pattern on RL is accounted for by using the integrated beam intensity at 3.5 kHz as a reference and therefore, RLs at 1.9 and 2.7 kHz, for example, are lowered by 3.2 and 1.5 dB, respectively.

ACKNOWLEDGMENT

The authors would like to thank the ONR, Ocean Acoustics, for sponsoring TREX13. The success of TREX13 was built on a collective effort from multiple institutions and multiple nations. These institutions include the Applied Physics Laboratory at the University of Washington (APL-UW); the Applied Research Laboratory, Pennsylvania State University; the Applied Research Laboratory at the University of Texas, Austin; the Scripps Oceanographic Institute; and Portland State University from the United States; DRDC from Canada, National University of Singapore; and NEUC from Italy. The authors would also like to thank the engineering personnel for their dedication and diver support at APL-UW, and Dale D. Ellis for hypothesizing the correlation between *RL* fluctuation and bottom bathymetry during the sea trial. The success of TREX13 also relies on the effort and coordination among multiple research vessels and

their crew members including the *R/V Sharp*, *R/V Quest*, and *R/V W. Smith*.

Reference

[1] C. F. Eyring, "Reverberation in the sea," *J. Acoust. Soc. Amer.*, vol. 20, pp. 462–475, 1948.

[2] R. J. Urick, "Side scattering of sound in shallow water," *J. Acoust. Soc. Amer.*, vol. 32, pp. 351–355, 1960.

[3] K. V. MacKenzie, "Bottom reverberation for 530- and 1030-cps sound in deep water," *J. Acoust. Soc. Amer.*, vol. 33, pp. 1498–1504, 1961.

[4] A. B. Baggeroer and J. A. Orcutt, "An overview of the 1991 reconnaissance cruise of the acoustic reverberation special research program," in *Ocean Reverberation*, D. D. Ellis, J. R. Preston, and H. G. Urban, Eds. Dordrecht, The Netherlands: Springer, 1993.

[5] N. C. Makris and J. M. Berkson, "Long range backscatter from the Mid-Atlantic Ridge," *J. Acoust. Soc. Amer.*, vol. 95, pp. 1865–1881, 1994.

[6] K. B. Smith, W. S. Hodgkiss, and F. D. Tappert, "Propagation and analysis issues in the prediction of long-range reverberation," *J. Acoust. Soc. Amer.*, vol. 99, pp. 1387–1404, 1996.

[7] J. R. Preston, "Reverberation at the mid-atlantic ridge during the 1993 ARSRP experiment seen by R/V alliance from 200-1400 Hz and some modeling inferences," *J. Acoust. Soc. Amer.*, vol. 107, pp. 237–259, 2000.

[8] J. Sellschopp, "Environmental assessment prior to a naval exercise," *Naval Forces*, vol. 6, pp. 25–27, 1997.

[9] E. Pouliquen, A. D. Kirwan, R. T., Jr., Pearson, Eds., "Rapid environmental assessment," *SACLANTCEN Conf., Proc. Series CP-44, NATOSACLANT Undersea Res. Centre*, La Spezia, Italy, 1997.

[10] A. Trangeled, P. Franchi, and A. Berni, "Data communication and data fusion architecture for Rapid Response 96-98," Saclant Undersea Res., La Spezia, Italy, Rep. SR-296, Jun. 1999.

[11] D. D. Ellis, J. R. Preston, R. Hollett, and J. Sellschopp, "Analysis of towed array reverberation data from 160–4000 Hz during rapid response 97," SACLANT Undersea Res., La Spezia, Italy, Rep. SR-280, Jul. 2000.

[12] J. R. Preston and Dale D. Ellis, "Extracting bottom information from towed-array reverberation data Part I: Measurement methodology," *J. Marine Syst.*, vol. 78, pp. 359–371, 2009.

[13] C. W. Holland *et al.*, "Boundary characterization experiment series overview," *IEEE J. Ocean. Eng.*, vol. 30, no. 4, pp. 784–806, Oct. 2005.

[14] J. R. Preston, D. D. Ellis, and R. C. Gauss, "Geoacoustic parameter extraction using reverberation data from the 2000 boundary characterization experiment on the malta plateau," *IEEE J. Ocean. Eng.*, vol. 30, no. 4, pp. 709–732, Oct. 2005.

[15] J. R. Preston, "Using triplet arrays for broadband reverberation analysis and inversions," *IEEE J. Ocean. Eng.*, vol. 32, no. 2, pp. 879–896, Oct. 2007.

[16] P. Ratilal *et al.*, "Long-range acoustic imaging of the continental shelf environment: The acoustic clutter reconnaissance experiment 2001," *J. Acoust. Soc. Amer.*, vol. 117, pp. 1977–1998, 2005.

[17] A. J. Harding, M. A. H. Hedlin, and J. A. Orcutt, "Migration of backscatter data from the mid-Atlantic ridge," *J. Acoust. Soc. Amer.*, vol. 103, no. 4, pp. 1787–1803, 1998.

[18] S. P. Pecknold and C. D. S. Tollefsen, "Characterizing transmission loss variability during the target and reverberation experiment 2013," *IEEE J. Ocean. Eng.*., vol. 42, no. 4, pp. 1135–1145, Oct. 2017.

[19] D. Tang, B. T. Hefner, and D. R. Jackson, "Direct-path backscatter measurements along the main reverberation track of TREX13," *IEEE J. Ocean. Eng.*, 2018, to be published.

[20] P. H. Dahl and D. R. Dall'Osto, "Observations of sea-surface waves during the 2013 target and reverberation experiment (TREX13) and relation to midfrequency sonar," *IEEE J. Ocean. Eng.*, vol. 42, no. 2, pp. 250–259, Apr. 2017.

[21] C. De Moustier, "Persistence of sharp acoustic backscatter transitions observed in repeat 400 kHz multibeam echosounder surveys offshore Panama City, Florida, over 1 and 24 months," *J. Acoust. Soc. Amer.*, vol. 136, pp. 2267, 2014.

[22] B. T. Hefner, "Characterization of seafloor roughness to support modeling of mid-frequency reverberation," *IEEE J. Ocean. Eng.*, vol. 42, no. 4, pp. 1110–1124, Oct. 2017.

[23] J. A. Goff, "Seismic and core investigation off Panama City, Florida, reveals sand ridge influence on formation of the shoreface ravinement," *Continental Shelf Res.*, vol. 88, pp. 34–46, 2014.

[24] J. Yang and D. Tang, "Direct measurement of sediment sound speed and attenuation in the frequency band of 2–8 kHz at the target and reverberation experiment site," *IEEE J. Ocean. Eng.*, vol. 42, no. 4, pp. 1102–1109, Oct. 2017.

[25] D. M. Farrell, P. H. Dahl, and D. R. Dall'Osto, "The background noise environment during the 2013 target and reverberation experiment," *IEEE J. Ocean. Eng.*, vol. 42, no. 4, pp. 1088–1093, Oct. 2017.

[26] A. Penko, J. Calantoni, and B. T. Hefner, "Modeling and observations of sand ripple formation and evolution during TREX13," *IEEE J. Ocean. Eng.*, vol. 42, no. 2, pp. 260–267, Apr. 2017.

[27] H. Medwin and C. S. Clay, *Fundamentals of Acoustical Oceanography*, New York, NY, USA: Academic, 1998, p. 578.

[28] G. Haralabus and A. Baldacci, "Unambiguous triplet array beamforming and calibration algorithms to facilitate an environmentally adaptive active sonar concept," in *Proc. Oceans*, 2006, pp. 1–6.

[29] T. H. C. Herbers, S. Elgar, and R. T. Guza, "Directional spreading of waves in the nearshore," *J. Geophys. Res.*, vol. 104, pp. 7683–7693, 1999.

[30] D. E. Weston and J. Revie, "Fish echoes on a long-range sonar display," *J. Sound Vib.*, vol. 17, pp. 105–112, 1971.

[31] N. C. Makris, P. Ratilal, D. T. Symonds, S. Jagannathan, S. Lee, and R. W. Nero, "Fish population and behavior revealed by instantaneous continental shelf-scale imaging," *Science*, vol. 311, pp. 660–663, 2006.

[32] T. K. Stanton, "Broadband acoustic sensing of the ocean," *J. Mar. Acoust. Soc. Japan*, vol. 36, pp. 19–31, 2009.

[33] P. C. Hines, S. M. Murphy, D. A. Abraham, and G. B. Deane, "The dependence of signal coherence on sea surface roughness for high and low duty cycle sonars in a shallow water channel," *IEEE J. Ocean. Eng.*, vol. 42, no. 2, pp. 298–318, Apr. 2017.

[34] S. Steele and S. P. Pechnold, "Modelling backscatter at mid-frequencies from sandy sediment in the Northern Gulf of Mexico, USA," *Atlantic Geology*, vol. 51, no. 1, 2015, doi: 10.4138/atlgeol.2015.015.

[35] D. R. Dall'Osto and P. H. Dahl, "Observations of water-column and bathymetric effects on the incident acoustic field associated with shallow water reverberation experiments," *IEEE J. Ocean. Eng.*, vol. 42, no. 4, pp. 1146–1161, Oct. 2017.

[36] J. Yang, D. R. Jackson, and D. Tang, "Mid-frequency geoacoustic inversion using bottom loss data from the shallow water 2006 experiment," *J. Acoust. Soc. Amer.* vol. V131, no. 2, pp. 1711–1721, 2012.

[37] D. D. Ellis, "Effect of cardioid and limaçon directional sensors on towed array reverberation response," *Can. Acoust.*, vol. 34, no. 3, pp. 102–103, 2006.

Jie Yang received the B.S. degree in physics from the Ocean University of Qingdao, Qingdao, China, in 1999 and the Ph.D. degree in mechanical engineering from Georgia Institute of Technology, Atlanta, GA, USA, in 2007.

Since 2007, she has been a Postdoctoral Fellow supported by the U.S. Office of Naval Research and currently a Principle Physicist at the Applied Physics Laboratory, University of Washington, Seattle, WA, USA. Her research interests include both active and passive acoustics, with the former focusing on mid-frequency sound propagation and reverberation in littoral oceans and the latter on estimating wind speed and rainrate using ocean ambient sound and their relation to global water cycle and climate change.

Dr. Yang is a member of the Acoustical Society of America.

Dajun Tang received the B.S. degree from the University of Science and Technology, Hefei, China, in 1981, the M.S. degree from the Institute of Acoustics, Beijing, China, in 1985, both in physics, and the Ph.D. degree in oceanographic engineering from the Joint Program of Massachusetts Institute of Technology, Cambridge, MA, USA, and the Woods Hole Oceanographic Institution, Woods Hole, MA, USA, in 1991.

From 1991 to 1996, he was first an Assistant Scientist and then an Associate Scientist at Woods Hole Oceanographic Institution. In 1996, he moved to the Applied Physics Laboratory, University of Washington, Seattle, WA, USA, where he is currently a Principal Senior Oceanographer. His research encompasses acoustics in shallow water, including both field experiments and modeling, whereas his current research interest is in the area of environmental impact on midfrequency reverberation.

Dr. Tang was a Co-Chief Scientist for the Shallow Water 2006 (SW06) experiment and the Target and Reverberation Experiment (TREX13). He is a Fellow of the Acoustical Society of America.

Brian T. Hefner received the B.S. degree in physics from Bard College, Annandale-On-Hudson, NY, USA, in 1994 and the M.S. and Ph.D. degrees in physics from Washington State University, Pullman, WA, USA, in 1996 and 2000, respectively.

From 2000 to 2001, he was a Postdoctoral Scholar at Crocker Nuclear Laboratory, University of California, Davis, CA, USA, where he studied light scattering from airborne dust using light detection and ranging. In 2001, he moved to the Applied Physics Laboratory, University of Washington, Seattle, WA, USA, where he is currently a Principal Physicist at the Department of Acoustics. His primary research interests include acoustic interaction with the seafloor, propagation and reverberation in shallow water, and sediment acoustics.

Dr. Hefner is a member of the Acoustical Society of America. He was a recipient of the A.B. Wood Medal from the Institute of Acoustics, St Albans, U.K., with the recommendation of the Acoustical Society of America, in 2013. He was a Co-Chief Scientist for the 2013 Target and Reverberation Experiment (TREX13).

Kevin Williams received the B.S., M.S., and Ph.D. degrees in physics from Washington State University, Pullman, WA, USA, in 1979, 1983, and 1985, respectively.

From 1985 to 1988, he was with the Naval Coastal Systems Center, Panama City, FL, USA, where his primary focus was in acoustic scattering from finite bodies and propagation into ocean sediments. In 1988, he moved to the Applied Physics Laboratory, University of Washington, Seattle, WA, USA, where he has worked in the area of high-frequency environmental acoustics (studying propagation through ocean internal waves and arctic ice and propagation in and scattering from ocean sediments) and understanding the response of targets in the ocean environment.

Dr. Williams is a Fellow of the Acoustical Society of America.

John R. Preston (M'76) received the B.S. degree in physics from the University of Massachusetts, Amherst, MA, USA, in 1967, the M.S. degree also in physics from the University of Maryland, College Park, MD, USA, in 1973, the M.S.E.E. degree in physics from George Washington University, Washington, DC, USA, in 1981, and the Ph.D. degree in acoustics from Pennsylvania State University, State College, PA, USA, in 2002.

Since 1995, he has been a Senior Research Associate at the Applied Research Laboratory, University of Texas, Austin, TX, USA, and Pennsylvania State University, State College, PA, USA. He is currently with the Acoustic Clutter Program, U.S. Office of Naval Research (ONR), Arlington, VA, USA, on the inversion algorithms with the U.S. Naval Air Warfare Center (NAWC) and the ONR, and with NATO Undersea Research Centre (NURC) on rapid environmental assessment (REA) technology. These efforts are focused on understanding sea bottom reverberation and clutter. He has also worked on broadband underwater propagation issues. From 1989 to 1994, he was with NURC, La Spezia, Italy, where he planned, executed, analyzed, and led various reverberation experiments using acoustic arrays. Before, he was a Vice President at Amron Corporation, Washington, DC, USA, where he worked on problems associated with underwater propagation and signal processing.

Dr. Preston is a member of the Acoustical Society of America.